## Title

Comparison of Big-Leaf, Two-Big-Leaf, and Two-Leaf Upscaling Schemes for Evapotranspiration Estimation Using Coupled Carbon-Water Modeling



## Journal

Journal of Geophysical Research Biogeosciences, 123(1)

## ISSN

2169-8953

## Authors

Luo, Xiangzhong
Chen, Jing M
Liu, Jane
et al.

## Publication Date

2018

## DOI

10.1002/2017jg003978

Peer reviewed

# Comparison of Big-Leaf, Two-Big-Leaf, and Two-Leaf Upscaling Schemes for Evapotranspiration Estimation Using Coupled Carbon-Water Modeling

Xiangzhong Luo[1,2], Jing M. Chen[1], Jane Liu[1,3], T. Andrew Black[4], Holly Croft[1], Ralf Staebler[5], Liming He[1], M. Altaf Arain[6], Bin Chen[1,7], Gang Mo[1], Alemu Gonsamo[1], and Harry McCaughey[8]

[1] Department of Geography and Planning, University of Toronto, Toronto, Ontario, Canada, [2] Lawrence Berkeley National Laboratory, Berkeley, CA, USA, [3] School of Atmospheric Sciences, Nanjing University, Nanjing, China, [4] Faculty of Land and Food Systems, University of British Columbia, Vancouver, British Columbia, Canada, [5] Air Quality Processes Research Section, Environment Canada, Toronto, Ontario, Canada, [6] School of Geography and Earth Sciences and McMaster Centre for Climate Change, McMaster University, Hamilton, Ontario, Canada, [7] International Institute for Earth System Science, Nanjing University, Nanjing, China, [8] Department of Geography, Queen's University, Kingston, Ontario, Canada

Correspondence to: X. Luo and J. M. Chen, xiangzhong.luo@mail.utoronto.ca; jing.chen@utoronto.ca

## Abstract

Evapotranspiration (ET) is commonly estimated using the Penman-Monteith equation, which assumes that the plant canopy is a big leaf (BL) and the water flux from vegetation is regulated by canopy stomatal conductance ($G_s$). However, BL has been found to be unsuitable for terrestrial biosphere models built on the carbon-water coupling principle because it fails to capture daily variations of gross primary productivity (GPP). A two-big-leaf scheme (TBL) and a two-leaf scheme (TL) that stratify a canopy into sunlit and shaded leaves have been developed to address this issue. However, there is a lack of comparison of these upscaling schemes for ET estimation, especially on the difference between TBL and TL. We find that TL shows strong performance ($r^2$ = 0.71, root-mean-square error = 0.05 mm/h) in estimating ET at nine eddy covariance towers in Canada. BL simulates lower annual ET and GPP than TL and TBL. The biases of estimated ET and GPP increase with leaf area index (LAI) in BL and TBL, and the biases of TL show no trends with LAI. BL miscalculates the portions of light-saturated and light-unsaturated leaves in the canopy, incurring negative biases in its flux estimation. TBL and TL showed improved yet different GPP and ET estimations. This difference is attributed to the lower $G_s$ and intercellular $CO_2$ concentration simulated in TBL compared to their counterparts in TL. We suggest to use TL for ET modeling to avoid the uncertainty propagated from the artificial upscaling of leaf-level processes to the canopy scale in BL and TBL.

## 1 Introduction

Land surface evapotranspiration (ET) plays a critical role in the water and energy exchanges between the biosphere and the atmosphere. It accounts

for 60% of the terrestrial precipitation (Oki & Kanae, 2006) and consumes 50% of the solar energy absorbed by the land surface (Trenberth et al., 2009). In the past decades, the Penman-Monteith (PM) equation has provided a sound foundation for estimating ET from the site to the global scales (Bonan, 1996; Dickinson et al., 1993; Moran et al., 1996; Mu et al., 2011; Sellers et al., 1986; Wang & Dickinson, 2012; Weiß & Menzel, 2008).

The PM equation perfectly combines the physical constraints and the biophysical constraints into one simple equation for ET estimations (Monteith & Unsworth, 2013). However, the simplicity of the PM equation also leads to a potential imperfection: in order to calculate canopy conductance ($G_c$), the PM equation has to use a big leaf assumption, which abstracts the whole canopy into a one-layer source. This assumption is in conflict with the complex structures of canopies in reality, where the leaf distribution varies by clumping (Chen et al., 1997), light environments (Norman, 1982), leaf angles and canopy heights (Baldocchi & Meyers, 1998), and consequently influence the canopy transpiration rates.

However, a considerable number of studies have used $G_c$ to produce reliable ET results regardless of the potential defect of the PM equation, hence corroborated the validity of the big-leaf scheme (BL) underlying the PM equation (Dickinson et al., 1991; Monteith & Unsworth, 2013; Moran et al., 1996; Mu et al., 2011; Yan et al., 2012). These studies regarded ET as an independent process, and $G_c$ for the PM equation can be freely tuned with experience to fit the ET measurements. $G_c$ is usually acquired through either a top-down or a bottom-up method. In the top-down method, $G_c$ is derived by inverting the PM equation using near-surface measurements of the latent heat flux and meteorological variables (Kelliher et al., 1995; Lai et al., 2000; Monteith & Unsworth, 2013; Phillips & Oren, 1998; Stewart, 1988). The reciprocal of $G_c$ value represents the bulk resistance enforced collectively by leaf stomata and soil to transport water (Paw & Meyers, 1989; Raupach & Finnigan, 1988). Process models used for large-scale ET simulations are often equipped with the bottom-up method, which identifies “two layers” for ET, namely, the transpiration from vegetation and the evaporation from soil. An integrated canopy stomatal conductance ($G_s$) is used to represent the control of vegetation in such two-layer models (Norman et al., 1995). Several theoretical and experimental studies have suggested that $G_s$ is not equivalent to $G_c$, though the value of $G_s$ would be close to $G_c$ for dense vegetation (Baldocchi & Meyers, 1998; Kelliher et al., 1995). $G_s$ is directly used in the PM equation to calculate canopy transpiration.

However, with the emergence of process-based Terrestrial Biosphere models (TBMs) that consider carbon and water exchange as a coupled process, $G_s$ acquired from BL should be able to satisfy the simulation of ET as well as the simulation of carbon uptake. The statistical model or semiempirical models that quantify $G_c$ or $G_s$ by inversing ET measurements or using empirical indices would no longer suffice for TBMs. The concept of $G_c$ and $G_s$ may not be appropriate anymore because photosynthesis model (Farquhar et al.,

1980) is only developed for leaves not for canopies. Ball et al. (1987) and Leuning (1990) discovered that stomatal conductance ($g_s$) is linearly tuned by the carbon assimilation rate ($A$) of leaves, denoted “Ball-Woodrow-Berry model” here. Sellers et al. (1992) and Amthor (1994) made the first efforts to update BL for TBMs. They assumed that $A$ decreases from the top to the bottom of a canopy following either the foliage nitrogen gradient or long-term solar radiation gradient, and so does $g_s$. These gradients are expressed in a form of an exponential function dependent on the canopy depth which is quantified using the accumulated LAI from the canopy top. Afterward, the canopy total photosynthesis ($A_c$, aka GPP (gross primary productivity)) can be easily upscaled from $A$ using these functions and then $G_s$ is calculated through the Ball-Woodrow-Berry stomatal conductance model.

BL designed for the carbon-water coupled TBMs was shown to perform well at some sites, but many researchers reported an underestimation of GPP by these models, since $A$ is more sensitive to the instantaneous solar radiation on leaves, while nitrogen and the long-term radiation gradient cannot explain the rapid changes in $A$ as described in BL (De Pury & Farquhar, 1997; Friend, 2001). For example, a leaf at the bottom of a canopy in a sun fleck will instantaneously receive far more radiation for photosynthesis than the average radiation that Beer's law would predict. To describe the instantaneous radiation intercepted by leaves, a two-leaf radiation regime was developed (Chen et al., 1999; De Pury & Farquhar, 1997; Norman, 1982; Sinclair et al., 1976). It separates a canopy into a group of sunlit leaves and a group of shaded leaves. $A$ of a sunlit leaf tends to be light saturated by receiving both direct and diffuse solar radiation, while $A$ of a shaded leaf is capped by the amount of diffuse radiation on leaves. Based on the two-leaf radiation regime, a hierarchy of upscaling schemes including the multilayer scheme, the two-big-leaf scheme (TBL), and the two-leaf scheme (TL) are developed for TBMs.

Leuning et al. (1995) and Baldocchi and Harley (1995) developed the multilayer scheme, in which a canopy is separated into layers, and every layer is divided into sunlit and shaded segments. The multilayer scheme considers the ecological processes inside the canopy in great detail: leaf nitrogen, leaf photosynthetic capacity, and even leaf inclination angles can be prescribed independently. In this scheme, the leaf photosynthesis and transpiration are calculated for each segment and then integrated into the canopy-scale GPP and ET by multiplying by the LAI of each segment. Though the multilayer scheme is regarded as the most accurate way to upscale fluxes from leaf to canopy, its expensive computational demand for large-scale applications drives the need to use simple upscaling schemes in TBMs (Wang & Leuning, 1998).

Some studies then developed an upscaling scheme which is classified as TBL, inheriting the idea of BL and using the two-leaf radiation regime (Dai et al., 2004; De Pury & Farquhar, 1997; Ryu et al., 2011; Wang & Leuning, 1998). $A_c$ and $G_s$ for sunlit and shaded canopies are simulated respectively in

TBL, and $G_s$ of each leaf group is then used in the PM equation to calculate ET. In order to calculate $A_c$ and $G_s$, TBL requires the biochemical parameters of leaves to be upscaled to their canopy counterparts. Since the biochemical model (i.e., Farquhar's biochemical model) is originally developed to simulate leaf-level photosynthesis, the direct application of it at the canopy scale can bring unexpected uncertainties in simulation when the physiological behavior of an imaginary “big leaf” surpasses the explanatory ability of a leaf-level model.

Chen et al. (1999, 2012) developed TL as an alternative to the multilayer scheme and TBL. TL separates the canopy into sunlit and shaded segments and calculate the $A$ and $g_s$ of a representative leaf for each segment. A representative leaf is the average status of all leaves in each segment. This method takes advantage of the two-leaf radiation regime and avoids the use of canopy parameters (i.e., $G_s$) in TBMs. It is conceptually rigorous in running the Farquhar's biochemical model, the Ball-Woodrow-Berry stomatal conductance model, and the PM equation simultaneously at the leaf level, since the first two were developed using leaf-level measurements.

Since the application of the two-leaf radiation regime in TBMs in 1990s, some studies have strived to evaluate the performance of different upscaling schemes with flux measurements. The advantage of TBL over BL has been proved at two flux sites for GPP modeling (Medlyn et al., 2003; Mercado et al., 2006), and TL has been validated with data from 11 eddy covariance (EC) towers and proved its advantage over BL on GPP modeling (Sprintsin et al., 2012). However, there is a lack of attention on the effects of upscaling schemes for ET simulations in carbon-water coupled models. Vogel et al. (1995) has used a TBM with the multilayer scheme to simulate ET and compared it with a hierarchy of less-sophisticated ET models over a well-irrigated cropland and suggested no advantage of using the two-leaf radiation regime for ET modeling. The conclusion may not be applicable for TBMs since the parameters for those less-sophisticated ET models can be freely tuned to fit the measurements, whereas the parameters of TBMs are simulated based on the physiological principle of carbon-water coupling. Currently, we still lack a clear understanding of the effects of upscaling schemes in TBMs for ET simulations and how these effects vary across sites. In addition, there is a need to clarify the definitions of the two-leaf radiation regime, TBL and TL, because of their interchangeable uses in previous studies (De Pury & Farquhar, 1997; Wang & Leuning, 1998). Therefore, the objective of this research is to compare BL, TBL, and TL over a spectrum of flux sites and analyze their influences on ET modeling.

## 2 Data and Method

### 2.1 Description of the Model

The Boreal Ecosystems Productivity Simulator (BEPS) is an enzyme kinetic, two-layer (i.e., vegetation and soil), and dual-source (sunlit and shaded) model first developed to estimate carbon uptake and the water cycle over

the Canadian landmass (Liu et al., 2003). It is characterized by a two-leaf radiation regime (Norman, 1982) and an analytic daily integration scheme (Chen et al., 1999). Several intermodel comparisons and site-level validations have shown that BEPS can produce reasonable GPP and ET estimates (Amthor et al., 2001; Grant et al., 2006; Liu et al., 2003; Potter et al., 2001). Its usage has expanded from boreal ecosystems to other plant functional types in the past decade (Chen et al., 2012; Gonsamo et al., 2013; Wang et al., 2004), and BEPS has been updated to support simulations at hourly and half-hourly steps (Chen et al., 2007).

In BEPS, ET from the land surface mainly consists of three components: transpiration from leaves, evaporation (sublimation) from the wet canopy, and evaporation (sublimation) from the soil surface. Since this study focuses on leaf-to-canopy upscaling methodologies and their effects on ET estimation, we will primarily describe the transpiration-related processes in BEPS.

According to TL, BEPS simulates the photosynthetic rate of a representative sunlit leaf ($A_{sunlit}$) and a shaded leaf ($A_{shaded}$) first and then obtains the canopy photosynthetic productivity ($A_c$) as the sum of the photosynthesis of leaves (equation 1). Similar to the calculation of $A_c$, the transpiration of the canopy ($T_c$) is the sum of transpiration from these two groups of leaves (equation 2). TL assumes that all sunlit leaves (shaded leaves) are exposed to the same environment (i.e., irradiance, temperature, and vapor pressure deficit) and have the same physiological features (i.e., $V_{max}^{25}$), and therefore, the transpiration and photosynthesis of the whole leaf group can be predicted using one representative leaf.

$$A_c = A_{sunlit} \times LAI_{sunlit} + A_{shaded} \times LAI_{shaded} \quad (1)$$

$$T_c = T_{sunlit} \times LAI_{sunlit} + T_{shaded} \times LAI_{shaded} \quad (2)$$

where $A_{sunlit}$ and $A_{shaded}$ are the photosynthetic rates of a representative sunlit leaf and a representative shaded leaf, respectively. They are acquired from an analytic solution derived from a leaf biochemical model and a mass transfer equation (Baldocchi, 1994). The maximum carboxylation velocity ( $V_{max}^{25}$) and the maximum electron transport capacity ( $J_{max}^{25}$) at 25°C for sunlit and shaded leaves are calculated based on a nitrogen gradient in the canopy (Appendix A) to parameterize the biochemical processes in BEPS. $T_{sunlit}$ and $T_{shaded}$ are the transpiration from sunlit leaf and shaded leaf, respectively. $LAI_{sunlit}$ and $LAI_{shaded}$ are the LAI of sunlit leaves and shaded leaves, respectively. The values of $LAI_{sunlit}$ and $LAI_{shaded}$ are calculated following the stratification scheme of Norman (1982) and Chen et al. (1999).

$$LAI_{sunlit} = 2\cos\theta(1 - \exp(-0.5\Omega LAI_{tot}/\cos\theta)) \quad (3)$$

$$LAI_{shaded} = LAI_{tot} - LAI_{sunlit} \quad (4)$$

where $\theta$ is the solar zenith angle, $LAI_{tot}$ is the total leaf area index of the canopy, and $\Omega$ is the clumping index.

Then, the PM equation is employed to calculate $T$ of a sunlit or shaded leaf (equation 5).

$$T = \frac{\Delta(R_n - G) + \rho c_p \mathrm{VPD} g_v}{\Delta + \left(1 + \frac{g_v}{g_s}\right)\gamma} \times \frac{1}{\lambda} \quad (5)$$

where $\lambda$ is the latent heat of evaporation of water, $R_n$ is the net radiation at the leaf surface (Appendix B), $G$ is the heat storage of the leaf which can be neglected, $\rho$ is the density of air, $c_p$ is the specific heat of air, VPD is the vapor pressure deficit of the ambient air, $\gamma$ is the psychrometric constant, $g_V$ is leaf boundary layer conductance for water vapor, $\Delta$ is the slope of the saturation vapor pressure curve at air temperature, and $g_s$ is the stomatal conductance of the representative sunlit or shaded leaf.

A modified Ball-Woodrow-Berry model is then used to calculate the $g_s$ of sunlit or shaded leaves (Chen et al., 2012), respectively.

$$g_s = f_w\left(\frac{mA \cdot \mathrm{RH}}{C_s}\right) + g_0 \quad (6)$$

where $m$ is the dimensionless Ball-Woodrow-Berry coefficient set at 8 for $C_3$ plants, RH is the relative humidity, $C_s$ is the carbon dioxide concentration on the leaf surface, $g_0$ is the minimum conductance at night, and $A$ is the rate of photosynthesis (μmol/m$^2$/s) of the representative sunlit or shaded leaf. The variable $f_w$, which is the soil water stress factor, is added to overcome the inability of the Ball-Woodrow-Berry equation to close the stomata during drought spells. It is widely employed as a complementary parameter to represent the regulation of the conductance of water through stomata (Sala & Tenhunen, 1996; Xu & Baldocchi, 2003). BEPS has developed a mechanistic module to simulate soil moisture and $f_w$ (Ju et al., 2006). However, sometimes the performance of the soil moisture module is biased because the module requires accurate parameterization of soil texture for multiple layers. To minimize the possible deviations in $g_s$ caused by the soil moisture simulation, we replaced the soil moisture module with measured soil moisture in this study and applied a simple equation to calculate $f_w$ (Appendix C). The incorporation of measured surface soil moisture also reduces the errors in the estimates of surface evaporation. With this modification, the overall change in ET between schemes is mainly attributed to the transpiration, and in turn be attributed to the corresponding upscaling scheme.

## 3 Modeling Schemes

### 3.1 Big-Leaf Scheme

BL developed by Sellers et al. (1992) and Sellers (1997) is one of the first attempts to simulate water and carbon fluxes simultaneously, in which.

$$A_c = A_0 \times \frac{1 - \exp(-k \times \mathrm{LAI}_{\mathrm{tot}})}{k} \quad (7)$$

where $A_0$ is the photosynthetic rate of the leaves at the top of the canopy and $A_c$ is the total canopy photosynthesis rate. Since BL assumes an optimal nitrogen gradient following the long-term solar radiation gradient, $k$ is the extinction coefficient for both solar radiation and nitrogen gradients in a canopy and it is set as 0.5. After obtaining $A_c$, $G_s$ for the big leaf is then acquired using the Ball-Woodrow-Berry equation introduced in equation 6. To facilitate our analysis, $G_s$ is simplified into the form of

$$G_s = g_{s0} \times \frac{1 - \exp(-k \times \mathrm{LAI_{tot}})}{k} \quad (8)$$

where $g_{s0}$ is the stomatal conductance of the leaves on top of the canopy.

## 3.2 Two-Big-Leaf Scheme

TBL applies a different way of describe the dual sources than TL (Figure 1). TBL scheme requires an artificial upscaling of leaf-level physiological parameters $V_{\mathrm{max}}^{25}$ and $J_{\mathrm{max}}^{25}$ to their counterparts for each leaf group (i.e., $V_{\mathrm{max\,sunlit\,canopy}}^{25}$, $V_{\mathrm{max\,shaded\,canopy}}^{25}$, $J_{\mathrm{max\,sunlit\,canopy}}^{25}$, and $J_{\mathrm{max\,shaded\,canopy}}^{25}$). By incorporating these canopy-scale parameters into Farquhar's model and the Ball-Woodrow-Berry equation, we are able to obtain $A_c$ and $G_s$ for the sunlit and shaded leaf groups, respectively. For the purpose of this study, TBL is added to existing BEPS to compute the $G_s$ of sunlit leaves ($G_{s\_\mathrm{sunlit}}$) and $G_s$ of shaded leaves ($G_{s\_\mathrm{shaded}}$) (Dai et al., 2004; Ryu et al., 2011; Wang & Leuning, 1998). The calculation of the canopy-scale $V_{\mathrm{max}}^{25}$ in TBL is introduced in Appendix D.

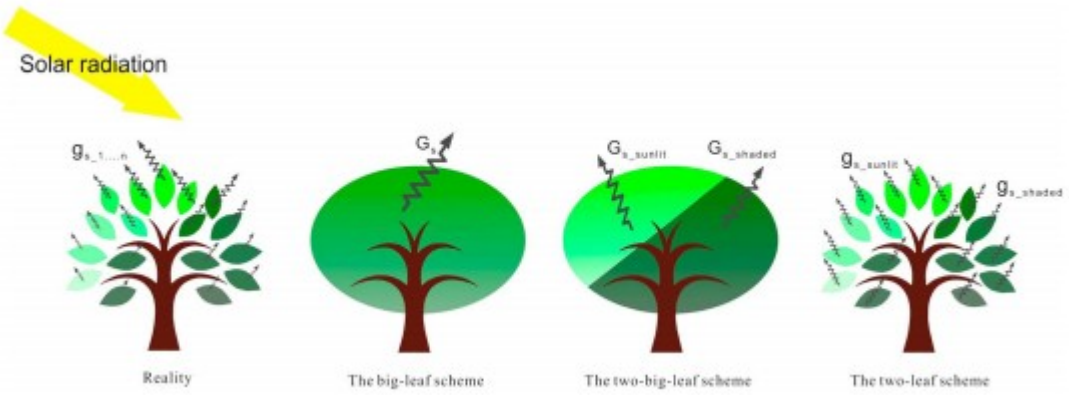


Figure 1

Schematic descriptions of the three upscaling schemes: BL, TBL, and TL. In reality, $g_s$ of each leaf is different. BL integrates $g_s$ into $G_s$; TBL integrates $g_s$ into $G_s$ for sunlit and shaded leaves, respectively; TL uses the average of $g_s$ of each leaf group and avoids the calculation of $G_s$.

## 3.3 Two-Leaf Scheme

The default BEPS uses TL to estimate the transpiration of a representative sunlit leaf and a representative shaded leaf first and then upscales the leaf-level transpiration to canopy level by multiplying by the corresponding LAI values (equation 2) (see section 2.1 for a more detailed description of TL). This method avoids the use of $G_s$ and canopy-level photosynthetic parameters, so it is described as TL.

## 4 Validation Sites and Input Data

The data used to drive the model are obtained from Fluxnet (http://fluxnet.ornl.gov/). Nine sites in Canada are selected, mainly because they have some measured leaf area index (LAI), clumping index (Ω), and soil moisture data (Table 1). Using these measurements can effectively constrain the uncertainty for ET simulation. The input meteorology data include incident solar irradiance ($W/m^2$), air temperature (°C), precipitation (mm/h), relative humidity (%), wind speed (m/s), and soil water content ($m^3/m^3$). Overstory LAI ($LAI_o$) data were measured during some growing seasons at these sites. We use the reflectance data of the Moderate-resolution Imaging Spectroradiometer to extrapolate the LAI measurements to daily $LAI_o$ sequences (Gonsamo & Chen, 2014). Except for an old aspen site (CaOas), the understorey LAI ($LAI_u$) is calculated using an empirical equation, $LAI_u = 1.18 \times e^{(-0.99 \times LAI_o)}$ (Liu et al., 2003). Since CaOas has an $LAI_u$ comparable to $LAI_o$ (Barr et al., 2004), its $LAI_u$ is calculated as 90% of $LAI_o$. The clumping index (Ω) is also a critical canopy structural parameter, as it defines the nonrandomness of the foliage distribution in a canopy (i.e., the overlapping of the leaves and aggregations of the needles in a shoot) (He et al., 2012). Ω ranges from 0 to 1, with a higher number indicating the canopy is closer to a random distribution.

**Table 1**
*Features of the Selected Canada Carbon Program Flux Tower Sites*

| Site code | Latitude | Longitude | Year | Land cover[a] | Overstorey main genera | Maximum over storey LAI[b] | Clumping index[c] | $V_{max}^{25}$ (μmol $m^{-2}$ $s^{-1}$)[f] | Number of LAI measurements | Reference |
|---|---|---|---|---|---|---|---|---|---|---|
| CaCa2 | 49.8705 | −125.2909 | 2002–2010 | ENF | *Pseudotsuga menziesii* | 4.45 | 0.48[d] | 38.8 | 26 | Chen et al. (2009) |
| CaCa3 | 49.5346 | −124.9004 | 2002–2010 | ENF | *Pseudotsuga Menziesii* | 8.15 | 0.532 | 38.8 | 31 | Chen et al. (2009) |
| CaCbo | 44.3185 | −79.9342 | 2008–2013 | DBF | *Acer rubrum, Populus tremuloides* | 4.96 | 0.72[e] | 62 | 30[h] | Froelich et al. (2015) |
| CaGro | 48.2173 | −82.1555 | 2005–2011 | MF | *Picea mariana* | 3.87 | 0.821 | 40 | 6 | Gökkaya et al. (2013) |
| CaOas | 53.6289 | −106.1978 | 2002–2010 | DBF | *Populus Tremuloides* | 2.43 | 0.87 | 62.5[g] | 9 | Barr et al. (2004) |
| CaObs | 53.9872 | −105.1178 | 2002–2010 | ENF | *Picea Mariana* | 3.45 | 0.662 | 39.4 | 6 | Bergeron et al. (2007) |
| CaOjp | 53.9163 | −104.6920 | 2005–2010 | ENF | *Pinus banksiana* | 2.01 | 0.599 | 31 | 12 | Barr et al. (2006) |
| CaTp3 | 42.7068 | −80.3483 | 2009–2013 | ENF | *Pinus strobus* | 7.17 | 0.518 | 31 | 15 | Peichl et al. (2010) |
| CaTp4 | 42.7098 | −80.3574 | 2009–2013 | ENF | *Pinus Strobus* | 8.10 | 0.513 | 31 | 15 | Arain and Restrepo-Coupe (2005) |

[a]The land cover type is adopted from the site introductions on the Fluxnet. The selected sites include deciduous broadleaf forests (DBF), evergreen needleleaf forests (ENF), and mixed forests (MF). [b]The maximum value of the available LAI measurements on the Fluxnet. These values refer total LAI of the overstorey. [c]Chen et al., (2006). [d]Canada Carbon Program. [e]He et al. (2012). [f]$V_{max}^{25}$ values refer to the maximum carboxylation capacity at 25°C for leaves on top of canopies, and they are derived based on the values provided by Groenendijk et al. (2011). We assume that same species should have similar $V_{max}^{25}$ values. For all the Douglas fir (*Pseudotsuga menziesii*) sites in British Columbia, $V_{max}^{25}$ ranges from 20.5 to 54.1 μmol $m^{-2}$ $s^{-1}$ (Groenendijk et al., 2011). In this study, the median $V_{max}^{25}$ (38.8 μmol $m^{-2}$ $s^{-1}$) of all these sites is assigned to site CaCa2 and CaCa3; CaCbo uses the average $V_{max}^{25}$ of all temperate deciduous forest; CaGro uses the average $V_{max}^{25}$ of all temperate mixed forest; CaObs uses the value that is provided. Since the dominate species of CaGro and CaObs are black spruce (*Picea mariana*), their $V_{max}^{25}$ should be similar. CaTp4 is the only pine (*Pinus*) site with a known $V_{max}^{25}$ of 31 μmol $m^{-2}$ $s^{-1}$. Since CaTp3 and CaOjp are also pine sites, they are also assigned a $V_{max}$ value of 31 μmol $m^{-2}$ $s^{-1}$. [g]He et al. (2014). [h]Croft et al. (2015).

$V_{max}^{25}$ is a critical parameter in Farquhar's photosynthesis model. $V_{max}^{25}$ for each site is obtained from previous data assimilation work (Groenendijk et al., 2011; He et al., 2014). The temporal variation in $V_{max}^{25}$ is also considered by assuming that the seasonal patterns of $V_{max}^{25}$ follows the season patterns of LAI (Ryu et al., 2011). In this study, the $V_{max}^{25}$ value on a given day in growing seasons is calculated using an empirical equation:

$$V^{25}_{\text{max\_day}} = \alpha \times V^{25}_{\text{max}} + (1-\alpha) \times V^{25}_{\text{max}} \times \frac{L_c - L_{\text{min}}}{\beta \times L_{\text{max}} - L_{\text{min}}} \quad (9)$$

where $L_{\text{max}}$, $L_{\text{min}}$, and $L_c$ are maximum, minimum, and current LAI values over the year, respectively. The empirical variables $\alpha$ and $\beta$ are set as 0.30 and 0.75, respectively. The ratio term $\frac{L_c - L_{\text{min}}}{\beta \times L_{\text{max}} - L_{\text{min}}}$ should range between 0 and 1.

## 5 Results

### 5.1 Difference Between Simulations and Measurements Among Three Schemes

Three versions of BEPS using different upscaling schemes (BL, TBL, and TL) are used to simulate ET and GPP at nine eddy covariance (EC) sites, and results from each scheme are evaluated against tower measurements (Figure 2 and Appendix E).

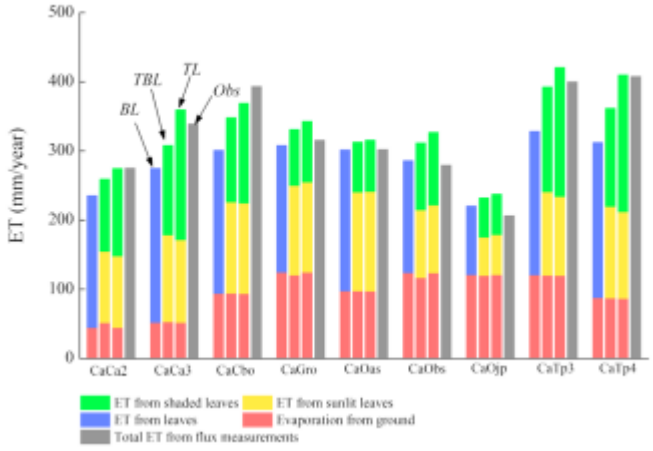


Figure 2

Simulated and measured annual ET at the studied sites, as well as the ET components obtained using BL, TBL, and TL.

According to Figure 2, the annual ET are 286 mm $yr^{-1}$, 318 mm $yr^{-1}$, 340 mm $yr^{-1}$, and 325 mm $yr^{-1}$ for BL, TBL, TL, and EC measurements across the sites, respectively. The annual ET estimated by BL and TBL are 16% and 7% lower compared to TL. BL, TBL, and TL produce similar evaporative fluxes from soil, indicating that soil evaporation is largely determined by the total radiation incident on the ground. Most of the difference between TL and TBL is caused by shaded leaves, where the average difference in ET estimates between TL and TBL is 24 mm $yr^{-1}$, while the difference between sunlit ET estimates of TBL and TL is only about −2 mm $yr^{-1}$.

Figure 3 demonstrates that GPP is underestimated by BL at all sites, while the GPP estimates from TBL and TL show a complex relationship. Five out of the nine sites have smaller GPP estimates from TBL than those from TL, while four sites show the opposite results. The pattern is clearer when partitioning GPP into its sunlit and shaded components: at eight out of the

nine sites, TL produces higher sunlit GPP than TBL; and at seven sites, shaded GPP from TL is smaller than that from TBL. Averaged across all sites, the total GPP are 922 g C $m^{-2}$ $yr^{-1}$, 1,250 g C $m^{-2}$ $yr^{-1}$, 1,232 g C $m^{-2}$ $yr^{-1}$, and 1,165 g C $m^{-2}$ $yr^{-1}$ for BL, TBL, TL, and EC measurements, respectively. Compared to TL, BL underestimates annual GPP by 25% and TBL overestimates GPP slightly by 1.5%.

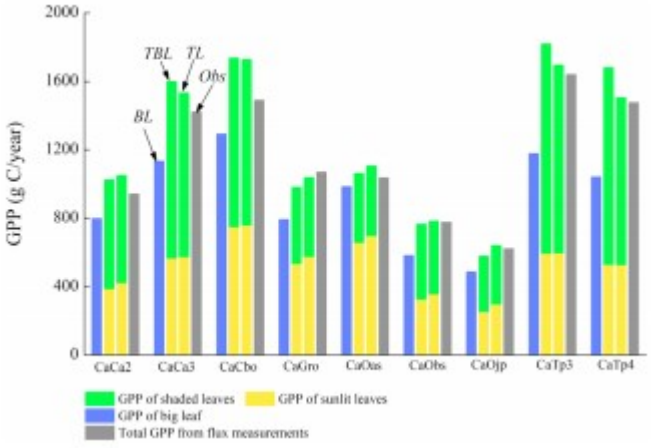


Figure 3

Simulated and measured annual GPP at the study sites, as well as the GPP components obtained using BL, TBL, and TL.

BL has been used in several carbon-water coupled TBMs (Alton et al., 2007; Cramer et al., 2001). Some studies have noticed the underestimation of GPP by BL, but the accompanying underestimation of ET has been less reported and inadequately studied across sites. The differences between the ET and GPP estimates by TL and TBL have not been studied as well. Figure 4 demonstrates the biases of annual ET and GPP estimates from BL, TBL, and TL and their relationships with LAI.

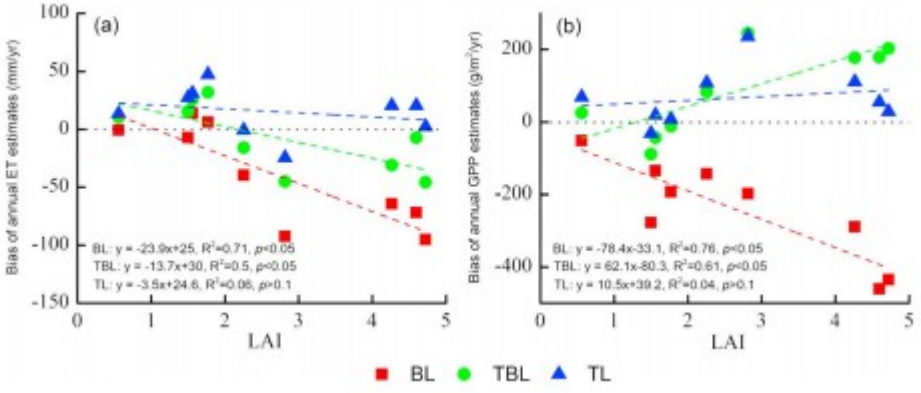


Figure 4

The biases of annual ET and GPP estimates along with site mean LAI for each upscaling scheme.

According to Figure 4, BL underestimates both GPP and ET, and TBL tends to underestimate ET but overestimate GPP. The biases in ET and GPP estimation by BL and TBL increase significantly ($p < 0.05$) with LAI, indicating that the sites with dense foliage tend to create large errors in ET and GPP estimates by BL and TBL. In contrast, the biases in ET and GPP estimation by TL are small and insensitive to LAI. For those low LAI sites, the difference between the simulations of TBL and TL are negligible, but their differences amplify with increasing LAI. These results suggest existence of errors in the modeling structures of BL and TBL that induce larger biases at higher LAI. In addition, the errors incurred by TBL are smaller than those by BL for ET and GPP estimation.

### 5.2 Difference Between the Radiation Regimes in BL and TBL (TL)

BL uses Beer's law to describe the radiation distribution inside a canopy, while TBL and TL both use the two-leaf radiation regime to describe the radiation distribution. The amount of intercepted radiation of leaves affects the photosynthetic rates of leaves and consequently influences conductance and ET. Figure 5 demonstrates the amount of light-saturated leaves for a given sunny day at the nine sites.

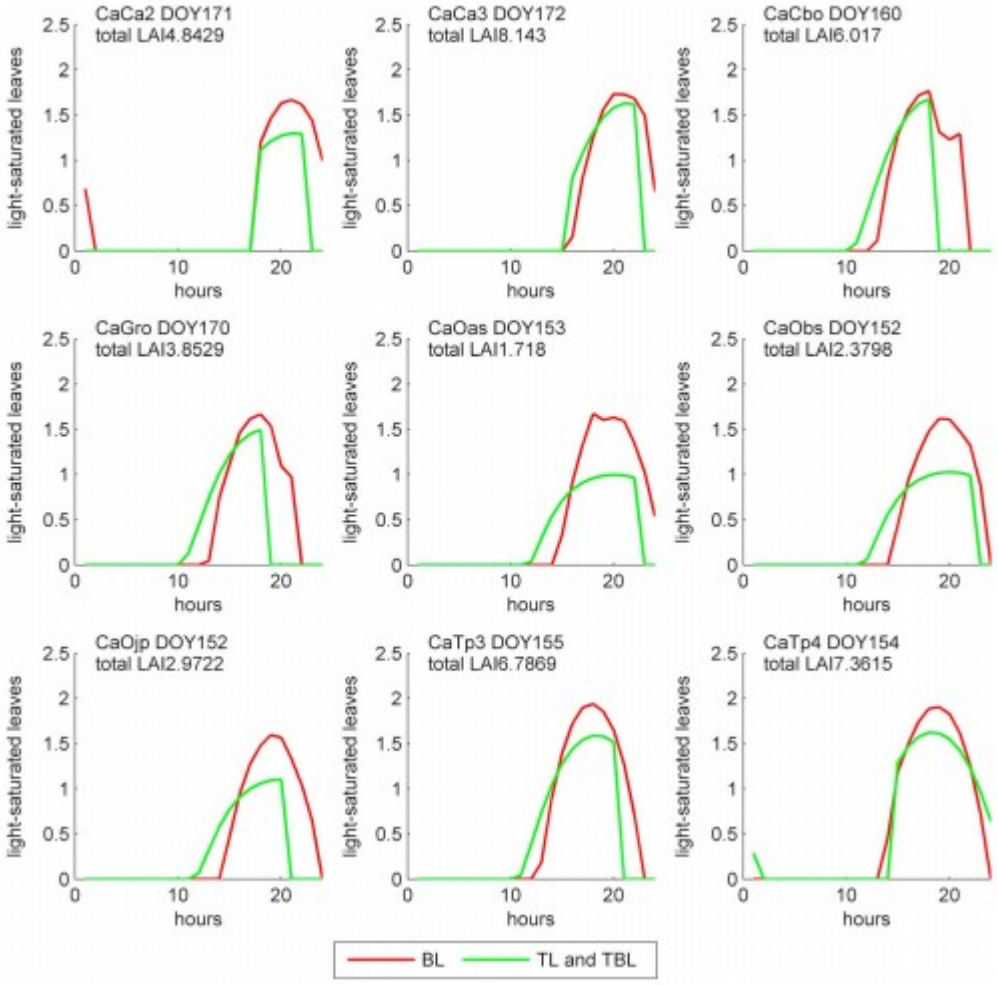


Figure 5

The amount of light-saturated leaves (LAI) at each site using BL and TBL (TL). The light saturation point is fixed at 400 W/m$^2$ for this analysis. coordinated universal time (UTC) is used for abscissas.

Figure 5 shows that BL usually classifies more leaves as light-saturated leaves than TBL and TL. Considering that light-saturated leaves have high photosynthetic rates, the GPP and ET contributed by light-saturated leaves are larger in BL than in TBL and TL. However, the total GPP and ET estimates are smaller in BL than in TBL and TL according to Figures 2-4, indicating that the underestimation in BL are mainly attributed to the underestimation of fluxes from light-unsaturated leaves. Light-unsaturated leaves includes all shaded leaves and the sunlit leaves with low solar irradiance. Because high LAI often indicates high percentage for shaded leaves, the underestimation of fluxes in BL increases with LAI.

## 5.3 Difference Between TBL and TL

TBL and TL both implement the two-leaf radiation regime, so the differences in their ET and GPP estimation are not caused by the simulation of radiation. Though TBL tends to simulate lower total ET and higher total GPP relative to

TL, we found that the sunlit and shaded parts of the canopies are affected differently using TBL (Figure 6).

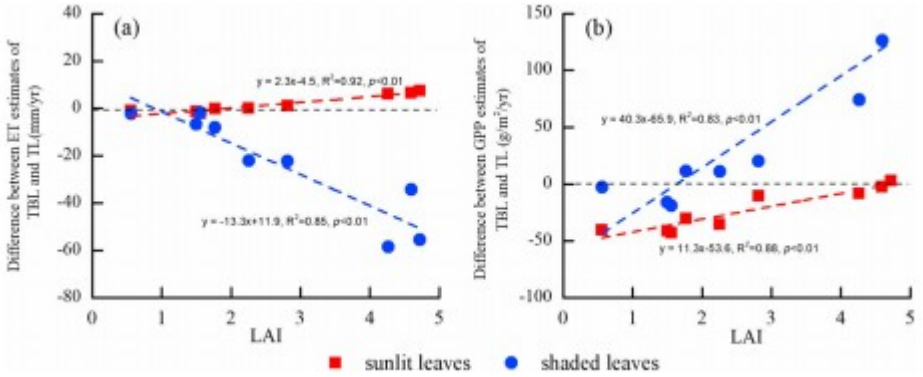


Figure 6

The differences in (a) ET and (b) GPP estimation between TBL and TL for sunlit and shaded leaves. Negative values mean TBL underestimates fluxes relatively to TL; positive values mean TBL overestimates fluxes relatively to TL.

Figure 6 demonstrates that for sunlit leaves, ET estimated by TBL and TL are similar to each other, while sunlit GPP is underestimated by TBL relative to estimates of TL. For shaded leaves, TBL underestimates ET at all sites with the ET underestimation amplifying with LAI. TBL overestimates shaded GPP at five sites and underestimates at four sites, and the difference between the GPP estimates of TBL and TL displays significant correlation with LAI. The difference between the estimated GPP and ET for shaded leaves is more pronounced than that for sunlit leaves.

In order to identify the reasons for the different estimates between TBL and TL, the simulation of ET is expressed in the form of diffusion equations:

$$ET_{TBL\_j} = G_{s\_j} \times (e_s - e_a) \quad (10)$$

$$ET_{TL\_j} = ET_{leaf\_j} \times LAI_j = g_{s\_j} \times (e_s - e_a) \times LAI_j \quad (11)$$

and for GPP simulation these equations are

$$GPP_{TBL\_j} = G_{s\_j} \times (C_a - C_i) \quad (12)$$

$$GPP_{TL\_j} = GPP_{leaf\_j} \times LAI_j = g_{s\_j} \times (C_a - C_i) \times LAI_j \quad (13)$$

where $j$ refers to sunlit or shaded leaves, $e_a$ is the atmospheric water vapor pressure, $e_s$ is the saturated water pressure in plant cells, $C_a$ is the atmospheric $CO_2$ concentration, and $C_i$is the intercellular $CO_2$ concentration.

According to equations 10 and 11, the difference between the ET estimates of TBL and TL is driven by the difference between $G_s$ and the value of $g_s \times$ LAI. Figure 7 compares $G_s$ values from TBL with the corresponding $g_s \times$ LAI values from TL for all nine sites.

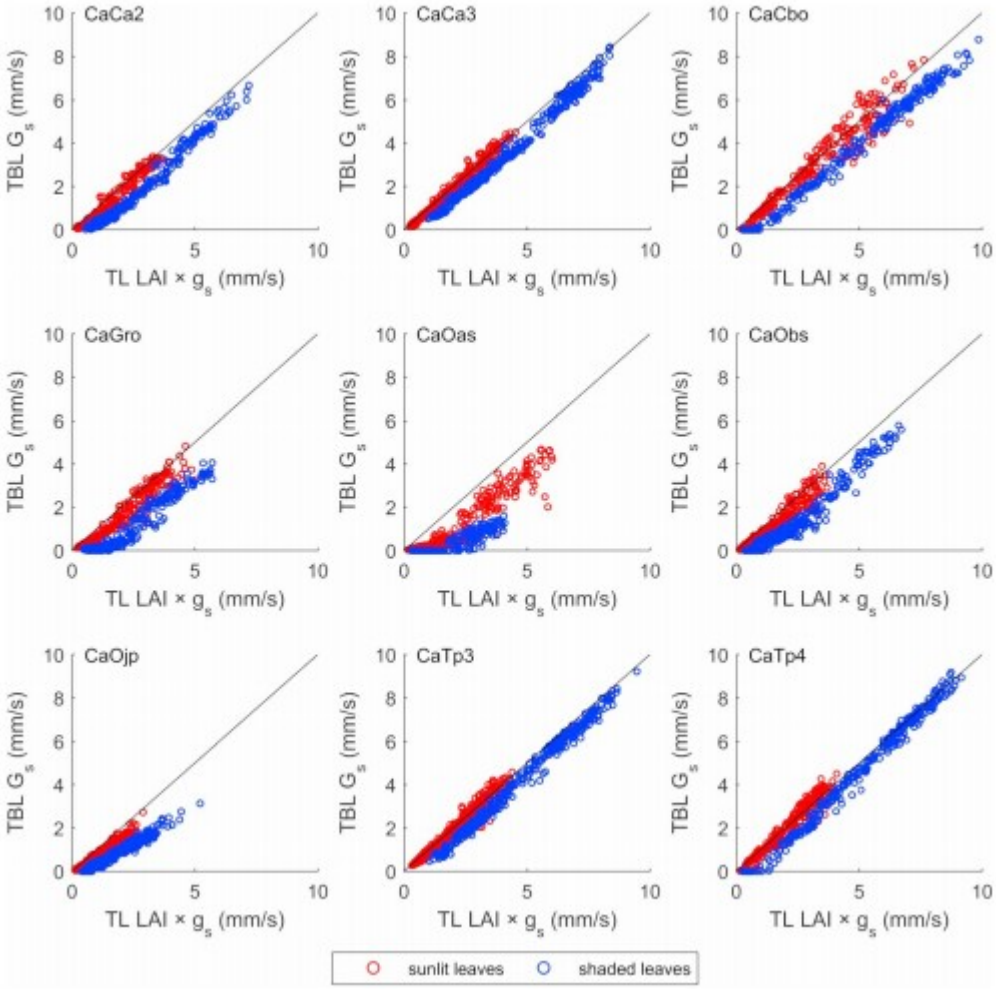


Figure 7

Comparison between the average daytime $G_s$ obtained from TBL and the $g_s$ × LAI obtained from TL for sunlit and shaded leaves.

Figure 7 shows that the TBL $G_s$ is smaller than the $g_s$ × LAI obtained from TL. Shaded leaves generally show larger gaps between TBL $G_s$ and the corresponding TL $g_s$ × LAI value than sunlit leaves. The difference between the $G_s$ and the $g_s$ × LAI suggests a potential caveat in the process of calculating $G_s$ in TBL. The relatively low value of $G_s$ in TBL could cause an underestimation of GPP and ET relative to TL.

However, Figure 6 has shown that TBL only underestimates ET for shaded leaves and GPP for sunlit leaves, while shaded GPP are sometimes even overestimated by TBL. This conflict indicates that there is another factor that drives the difference between TL and TBL for GPP simulation. Based on equations 12 and 13, we expect the $C_i$ values estimated by TL and TBL are different (Figure 8).

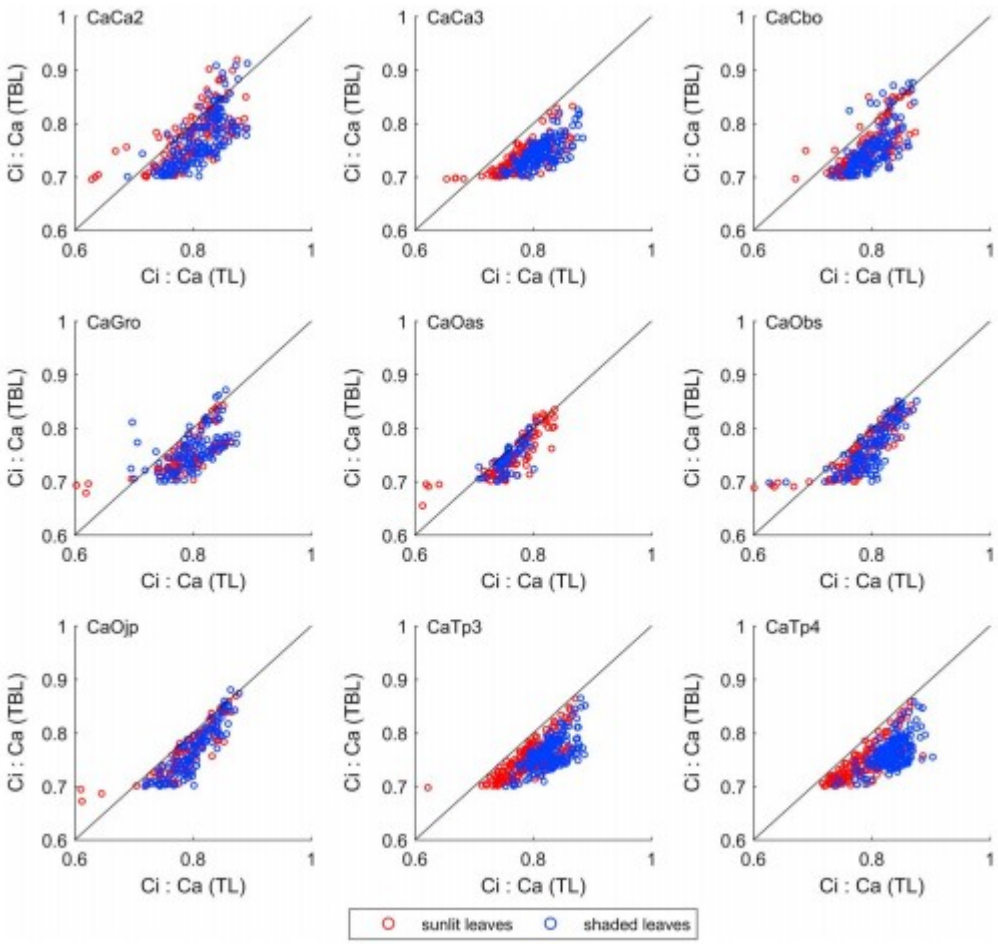


Figure 8

Comparison between the daytime average $C_i$:$C_a$ obtained from TBL and TL for sunlit and shaded leaves.

Figure 8 shows that $C_i$ simulated by TBL is smaller than that of TL for both sunlit and shaded leaves. The smaller $C_i$ in TBL leads to a greater gradient to drive the $CO_2$ to diffuse from the atmosphere to the inside of leaves and consequently compensates for the underestimation of $G_s$ in TBL for GPP estimations. In addition, the underestimation of $C_i$ by TBL is usually stronger at sites with large LAI values (e.g. CaCa3, CaTp3, and CaTp4), and thus, this compensation effect at those sites is even able to incur the overestimations of GPP by TBL (Figure 4).

## 6 Discussion

For the first time, our results demonstrate the differences between TBL and TL in estimating biosphere-atmosphere carbon and water exchanges. The underestimations of $G_s$ and $C_i$ in TBL are responsible for the difference between the fluxes estimated by TBL and TL. The structure of TL and TBL models is briefly demonstrated in Figure 9 to explore the driver for the underestimations of $G_s$ and $C_i$ in TBL.

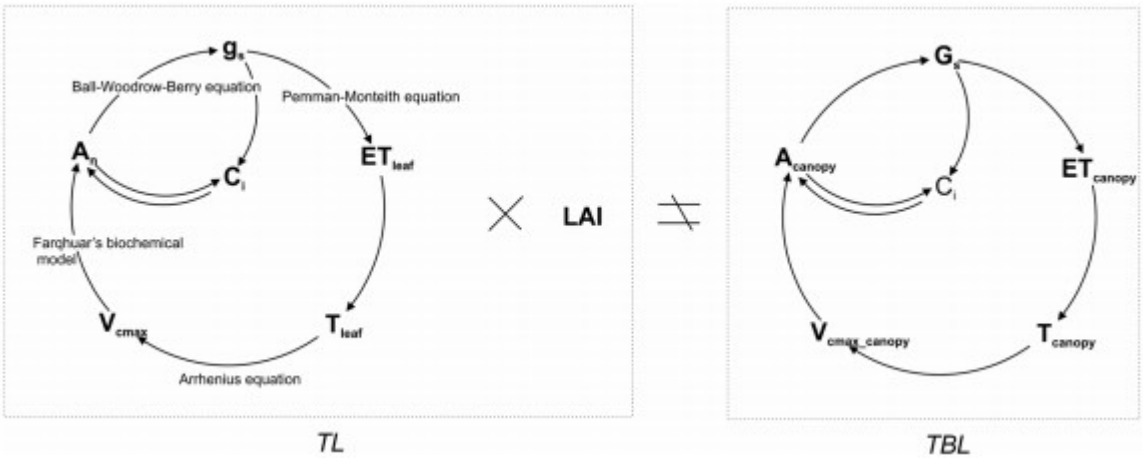


Figure 9

A schematic description of the difference between TL and TBL models. The nonlinear processes in models determine that the product of $g_s$ from TL and LAI does not equal to $G_s$from TBL, for either sunlit or shaded leaves.

Process-based TBMs usually consider various linear and nonlinear biochemical and biophysical processes in simulating GPP and ET (Figure 9). In TL, all these processes are performed at the leaf level, then the estimated fluxes of leaves are upscaled to the canopy scale by timing LAI. In TBL, these processes are simulated at the canopy scale through upscaling the key biochemical and biophysical parameters from leaf to canopy. If all the processes considered in TBMs were linear, TL would be equivalent to TBL, and $G_s = g_s \times$ LAI. However, due to Jensen's inequality, $G_s$ cannot be expressed as a linear function of $g_s$ and LAI.

$C_i$ is dynamically adjusted in plants shown in Figure 9 until the model realizes an optimal water use efficiency (WUE; Medlyn et al., 2011; Sellers, 1997; Wang et al., 2017). With an artificially upscaled $V_{max}^{25}$, a big leaf is apparently more capable of assimilating $CO_2$ compared to the leaves in reality in the same environment, and thus driving $C_i$ to be lower in the big leaf. With the change of photosynthesis by using the big leaf, the WUE is expected to be adjusted accordingly to obtain an optimal value. This big leaf WUE is different from the WUE acquired directly from leaf level simulations.

Figure 10 shows that the WUE acquired from TBL is similar to that from TL for sunlit leaves, while for shaded leaves the WUE acquired from TBL is larger than its counterpart in TL. Based on the separation of sunlit and shaded LAI described by equations 3 and 4, we know that the sunlit LAI could not be larger than 2 and the remaining LAI are assigned to shaded leaves. Therefore, the difference between the WUE of a shaded big leaf and a shaded leaf is stronger than that for sunlit leaves. The WUE estimated by TBL also is positively correlated with LAI, which may raise doubts on the analysis of WUE trend in the context of climate change using TBL.

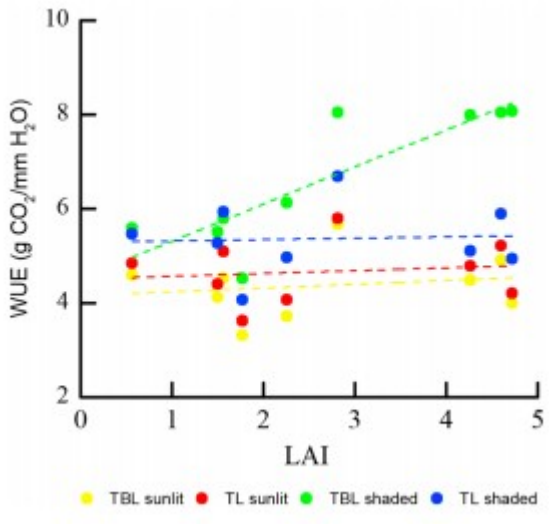


Figure 10

WUE for sunlit and shaded leaves estimated by TBL and TL.

At last, considering that most biochemical and biophysical processes in TBMs are originally developed based on leaf-level measurements, we suggest that it is conceptually correct to apply TL to TBMs which uses $g_s$ in the mathematical formulations of these processes and avoids the uncertainties propagated from the derivation of the canopy-scale parameters as intermediate variables. Though the results from TL models may not be superior to the results from TBL due to a range of reasons such as observational uncertainty of inputs, uncertainty of flux measurements, and the uncertainty of leaf-level parameters, the difference between the estimates from TBL and TL is worth noting since estimates from TBL show systematically increasing bias with LAI. With a given set of input parameters, the systematic differences between TL and TBL models at all test sites suggest that more attention should be given to model structure in addition to improving model parameters. In fact, using a model with correct structure and processes should be a prerequisite to tuning model parameters in the quest to understand the complex processes governing the carbon and water fluxes of terrestrial ecosystems.

## 7 Conclusion

The big leaf concept is widely used to describe the bulk control of plant canopies on transporting water and carbon molecules. It is characterized by the use of canopy conductance in the Penman-Monteith equation. In order to consider the physiological principle of carbon-water coupling, some state-of-the-art TBMs expand the big leaf concept by upscaling leaf-level photosynthetic parameters to their canopy-level counterparts, and directly using of leaf-level biochemical models at the canopy scale. $G_s$ is then calculated in BL for ET simulation. However, BL has been reported to incur some biases in GPP estimation, and TBL has been developed to address the problem (e.g., De Pury & Farquhar, 1997). Meanwhile, less attention has

been paid to the uncertainties underlying the artificial upscaling process for $G_s$ and other biochemical parameters in BL and TBL. In this study, we aim to promote the use of TL in TBMs built on the carbon-water coupling principle and to avoid the use of $G_c$ and $G_s$ in the Penman-Monteith equation. The performance of BL, TBL, and TL in estimating ET and GPP are evaluated with flux measurements from nine eddy covariance towers. Our conclusions are as follows:

1. BL underestimates ET and GPP across all sites because the radiation gradient calculated based on Beer's law fails to describe the instantaneous radiation distribution in the canopy. Increasing LAI leads to the increasing underestimations of ET and GPP in BL, mainly due to the underestimation of fluxes from shaded leaves.
2. TBL and TL demonstrate improved ET and GPP estimations by implementing the sunlit-shaded radiation regime. TBL and TL produce very similar total GPP and ET values when LAI is low but amplified difference when LAI is high. This difference is attributed to the lower $G_s$ and $C_i$ simulated in TBL than their counterparts in TL.
3. The nonlinear biophysical and biochemical processes make it questionable to use any form of big leaf (i.e., TBL and BL) in carbon-water coupled TBMs, through using $G_c$ or $G_s$. Conceptually, TL is appropriate for carbon-water coupled TBMs since it couples the water flow with the carbon flow at the leaf level by directly using the stomatal conductance derived from leaf biochemical models for ET modeling.

Acknowledgments

The authors wish to thank the efforts of researchers in Canadian Carbon Program for maintaining the sites and collecting data. This study is financially supported by a Discovery Grant and a Strategic Grant from the Natural Science and Engineering Research Council of Canada and a Canada Research Chair to J. M. Chen. L. He is supported by the Canadian Space Agency grant (14SUSMAPTO). We would like to thank Dennis Baldocchi for his insightful comments on the paper. The data used could be obtained from Fluxnet (http://fluxnet.ornl.gov/). The codes of BEPS model using BL, TBL, and TL are stored at https://github.com/JChen-UToronto/BEPS_H

Appendix A: Nitrogen-Weighted $V_{max}^{25}$ and $J_{max}^{25}$ for Sunlit and Shaded Leaves

Chen et al. (2012) combined the “two-leaf” separation scheme and a nitrogen gradient to derive the $V_{max}^{25}$ and $J_{max}^{25}$ values for the sunlit and shaded leaves separately. Leaf nitrogen content per leaf area $N(L)$ generally decreases exponentially from the top to the bottom in a canopy (equation A1):

$$N(L) = N_0 e^{-k_n L} \quad \text{(A1)}$$

where the extinction coefficient $k_n = 0.3$ used in BEPS is adopted from De Pury and Farquhar (1997), $N_0$ is the nitrogen content at top of the canopy,

and $L$ is the canopy depth described in total LAI. On the other hand, the leaf maximum carboxylation rate at 25°C ( $V_{max}^{25}$) is proportional to the leaf nitrogen content therefore it can be expressed as:

$$V_{max}^{25}(L) = V_{max\_0}^{25}\chi_n N(L) \quad \text{(A2)}$$

where $V_{max0}^{25}$ is the $V_{max}^{25}$ of the leaves at the top of the canopy and $\chi_n$ quantifies the relative change of $V_{max}^{25}$ to the leaf nitrogen content in the canopy. $\chi_n$ has units of $m^2/g$ while $N(L)$ has units of $g/m^2$. The value of $\chi_n$, the mean value of $N$ and its standard deviation, and the standard deviation of $V_{max}^{25}$ are provided according to the plant functional types (Chen et al., 2012). $N_0$ is taken as the mean $N$ value plus one standard deviation; $V_{max0}^{25}$ is taken as the input $V_{max}^{25}$ value plus one standard deviation.

The fraction of the sunlit and shaded leaves in the canopy change with the canopy depth:

$$f_{sun}(L) = \Omega e^{-kL} \quad \text{(A3)}$$

$$f_{sh}(L) = 1 - \Omega e^{-kL} \quad \text{(A4)}$$

where $k = G(\theta)\Omega/\cos\theta$. $G(\theta)$ is the projection coefficient of the canopy, and it is 0.5 assuming a spherical leaf angle distribution. Ω is the clumping index, and $\theta$ is the solar zenith angle. We assume the $V_{max}^{25}$ of a representative sunlit or shaded leaf is equal to the mean $V_{max}^{25}$ value of the sunlit or shaded leaves' group. Therefore, the $V_{max}^{25}$ of a representative sunlit or shaded leaf is obtained by the following integrations:

$$V_{max\_sunlit}^{25} = \frac{\int_0^L V_{max\_0}^{25}\chi_n N(L) f_{sun}(L)\mathrm{d}L}{\int_0^L f_{sun}(L)\mathrm{d}L} = V_{max\_0}^{25}\chi_n N_0 \frac{\int_0^L e^{-k_n L}\Omega e^{-kL}\mathrm{d}L}{\int_0^L \Omega e^{-kL}\mathrm{d}L} = V_{max\_0}^{25}\chi_n N_0 \frac{k\left[1 - e^{-(k_n+k)L}\right]}{(k_n+k)(1-e^{-kL})} \quad \text{(A5)}$$

$$V_{max\_shaded}^{25} = \frac{\int_0^L V_{max\_0}^{25}\chi_n N(L) f_{sh}(L)\mathrm{d}L}{\int_0^L f_{sh}(L)\mathrm{d}L} = V_{max\_0}^{25}\chi_n N_0 \frac{\int_0^L e^{-k_n L}\left(1 - \Omega e^{-kL}\right)\mathrm{d}L}{\int_0^L (1 - \Omega e^{-kL})\mathrm{d}L} = V_{max\_0}^{25}\chi_n N_0 \frac{\frac{1}{k_n}\left(1 - e^{-k_n L}\right) - \frac{\Omega}{k+k_n}\left[1 - e^{-} \right.}{L - 2\cos\theta(1 - e^{-kL})} \quad \text{(A6)}$$

After the $V_{max}^{25}$ values of the representative sunlit and shaded leaves are obtained, the maximum electron transport rate at 25°C ( $J_{max}^{25}$) is obtained using the following equations (Medlyn et al., 1999).

$$J_{max\_sunlit}^{25} = 2.39V_{max\_sunlit}^{25} - 14.2 \quad \text{(A7)}$$

$$J_{max\_shaded}^{25} = 2.39V_{max\_shaded}^{25} - 14.2 \quad \text{(A8)}$$

Appendix B: Leaf Energy Budget

In the absence of rainfall and snow coverage over leaves, the leaf energy budget is composed of the net radiation on leaf ($R_n$), the sensible heat ($Q$), and the latent heat (LE) from the leaf in every hourly step, during which period the heat storage of leaf is negligible.

$$R_n = H + \mathrm{LE} \quad \text{(B1)}$$

B1. Net Radiation on a Leaf

In BEPS the whole canopy was divided into four groups of leaves based on the location and radiation features of the leaves, namely, sunlit leaves in the overstorey, shaded leaves in the overstorey, sunlit leaves in the understorey, and shaded leaves in the understorey (Chen et al., 1999; Liu et al., 2003). The leaves in each group have identical features, so BEPS could use one leaf to represent a group. Net radiation on a leaf comprises three sources:

$$R_{n\_i} = R_{\mathrm{dir}\_i} + R_{\mathrm{dif}\_i} + R_{l\_i} \quad \text{(B2)}$$

where $R_n$ is the total net radiation on a given leaf, $R_{\mathrm{dir}}$, $R_{\mathrm{dif}}$, and $R_l$ refers to the net direct incoming solar radiation, net diffuse solar radiation, and net longwave radiation on the leaf. The subscript $i$ refers to one of the four types of leaves. For a shaded leaf, $R_{\mathrm{dir}} = 0$.

In order to differentiate the incoming solar radiation into a direct and diffuse part, a semiempirical equation is applied:

$$\frac{S_{\mathrm{dif}}}{S_g} = \begin{cases} 0.943 + 0.734r - 4.9r^2 + 1.796r^3 + 2.058r^4 & r < 0.8 \\ 0.13 & r \geq 0.8 \end{cases} \quad \text{(B3)}$$

$$S_{\mathrm{dir}} = S_g - S_{\mathrm{dif}} \quad \text{(B4)}$$

where $S_g$, $S_{\mathrm{dir}}$, and $S_{\mathrm{dif}}$ are incident solar irradiance, incoming direct solar radiation, and diffuse solar radiation, respectively. $r$ is a parameter used to quantify the cloudiness of the sky.

$$r = \frac{S_g}{S_0 \cos\theta} \quad \text{(B5)}$$

where $S_0$ is the solar constant set as 1,362 W/m$^2$ and $\theta$ is the solar zenith angle.

The net direct solar radiation on the sunlit representative leaf in the overstorey or understorey of the canopy is

$$R_{\mathrm{dir\_o\_sunlit}} = R_{\mathrm{dir\_u\_sunlit}} = (1 - \alpha_L) S_{\mathrm{dir}} \cos\alpha / \cos\theta \quad \text{(B6)}$$

where $\alpha_L$ is the albedo of the leaves. But in BEPS, $\alpha_L$ is different for the overstorey and the understorey because snow coverage varies with canopy depth. The parameter $\alpha$ is the mean leaf-sun angle which is fixed at 60° when the canopy has a spherical leaf distribution.

On the other hand, the net diffuse solar radiation on the four groups of the leaves are approximated, respectively, as

$$R_{\mathrm{dif\_o\_sunlit}} = R_{\mathrm{dif\_o\_shaded}} = (1 - \alpha_L)\left(S_{\mathrm{dif}}\left[1 - e^{-0.5\Omega \mathrm{LAI}_o / \cos\bar{\theta}_o}\right] / \mathrm{LAI}_o + C_{o.}\right) \quad \text{(B7)}$$

$$R_{\mathrm{dif\_u\_sunlit}} = \mathrm{R}_{\mathrm{dif\_u\_shaded}} = (1 - \alpha_L)\left(S_{\mathrm{dif}} e^{-0.5\Omega \mathrm{LAI}_o / \cos\bar{\theta}_o}\left[1 - e^{-0.5\Omega \mathrm{LAI}_u / \cos\bar{\theta}_u}\right] / \mathrm{LAI}_u + C_u\right) \quad \text{(B8)}$$

where $LAI_o$ and $LAI_u$ are the LAI value of the overstorey and the understorey and $C_o$ and $C_u$ are used to quantify the multiple scattering of the direct solar radiation from the leaf (Chen et al., 1999)

$$C_o = 0.07\Omega S_{dir}(1.1 - 0.1LAI)e^{-\cos\theta} \quad \text{(B9)}$$

$$C_u = 0.07\Omega S_{dir}e^{-0.5\Omega LAI_o/\cos\theta}(1.1 - 0.1LAI_u)e^{-\cos\theta} \quad \text{(B10)}$$

$\bar{\theta}_o$ and $\bar{\theta}_o$ are the representative zenith angles for diffuse radiation transmission of the overstorey and understorey leaves and slightly dependent on the corresponding LAI (Liu et al., 2003):

$$\cos\bar{\theta} = 0.537 + 0.025LAI \quad \text{(B11)}$$

The net longwave radiation on these leaves is calculated as

$$R_{L\_o\_sunlit} = R_{L\_o\_shaded} = \frac{1}{LAI_o}\left\{\left\{\varepsilon_o\left[\varepsilon_a\sigma T_a^4 + \varepsilon_u\sigma T_u^4\left(1 - e^{-0.5LAI_o\Omega/\cos\bar{\theta}_u}\right) + \varepsilon_g\sigma T_g^4 e^{-0.5LAI_u\Omega/\cos\bar{\theta}_u}\right] - 2\varepsilon_o\sigma T_o^4\right\}\left(1 - e^{-0.5LAI_o\Omega/\cos\bar{\theta}_o}\right) + \varepsilon_o(1-\varepsilon_u)\left(1 - e^{-0.5LAI_u\Omega/\cos\bar{\theta}_u}\right)\left[\varepsilon_a\sigma T_a^4 e^{-0.5LAI_o\Omega/\cos\bar{\theta}_o} + \varepsilon_o\sigma T_o^4\left(1 - e^{-0.5LAI_o\Omega/\cos\bar{\theta}_o}\right)\right]\right\} \quad \text{(B12)}$$

$$R_{L\_u\_sunlit} = R_{L\_u\_shaded} = \frac{1}{LAI_u}\left\{\left\{\varepsilon_u\left[\varepsilon_a\sigma T_a^4 e^{-0.5LAI_o\Omega/\cos\bar{\theta}_o} + \varepsilon_o\sigma T_o^4\left(1 - e^{-0.5LAI_o\Omega/\cos\bar{\theta}_o}\right) + \varepsilon_g\sigma T_g^4\right] - 2\varepsilon_u\sigma T_u^4\right\}\left(1 - e^{-0.5LAI_u\Omega/\cos\bar{\theta}_u}\right) + \varepsilon_u(1-\varepsilon_g)\left\{\left[\varepsilon_a\sigma T_a^4 e^{-0.5LAI_o\Omega/\cos\bar{\theta}_o} + \varepsilon_o\sigma T_o^4\left(1 - e^{-0.5LAI_o\Omega/\cos\bar{\theta}_o}\right)\right]e^{-0.5LAI_u\Omega/\cos\bar{\theta}_u} + \varepsilon_u\sigma T_u^4\left(1 - e^{-0.5LAI_u\Omega/\cos\bar{\theta}_u}\right)\right\} + \varepsilon_u(1-\varepsilon_o)\left[\varepsilon_u\sigma T_u^4\left(1 - e^{-0.5LAI_u\Omega/\cos\bar{\theta}_u}\right) + \varepsilon_g\sigma T_g^4 e^{-0.5LAI_u\Omega/\cos\bar{\theta}_u}\right]\left(1 - e^{-0.5LAI_o\Omega/\cos\bar{\theta}_o}\right)\right\} \quad \text{(B13)}$$

where $\sigma$ is the Stephen-Boltzmann constant equals to $5.67 \times 10^{-8}$ W m$^{-2}$ K$^{-4}$. $\varepsilon_a$, $\varepsilon_o$, $\varepsilon_u$, and $\varepsilon_g$ are the emissivity of the atmosphere, overstorey, understory, and ground surface, respectively. $\varepsilon_o$, $\varepsilon_u$, and $\varepsilon_g$ are prescribed as 0.98, 0.98, and 0.95, respectively, according to (Chen et al., 1989; Chen & Zhang, 1989), and $\varepsilon_a$ is computed as $\varepsilon_a = 1.24\left(\frac{e_a}{T_a}\right)^{1/7}$ (Brutsaert, 1982), where $e_a$ and $T_a$ are water vapor pressure in mbar and temperature of the atmosphere in $K$. $T_o$, $T_u$, and $T_g$ are the temperatures of the overstorey, the understorey, and ground, respectively, in kelvin, and $T_o$ and $T_u$ are calculated as the weighed average temperature of sunlit leaves and shaded leaves in overstorey and understorey, respectively.

## B2. Sensible Heat From a Leaf

The sensible heat is calculated for overstorey sunlit leaves, overstorey shaded leaves, understorey sunlit leaves, and understorey shaded leaves, respectively.

$$Q_i = (T_i - T_a)\rho c_p g_{H\_i} \quad \text{(B14)}$$

where $i$ refers to the type of the leaf, $\rho$ is the density of air, $c_p$ is the specific heat of air, and $g_H$ is total conductance of heat from the leaf surface to the atmosphere, which equals to the reciprocal of the leaf boundary layer resistance and aerodynamic resistance in tandem.

B3. Latent Heat From a Leaf

Latent heat is calculated using the Penman-Monteith equation (equation 5), which was simplified into a linear function of leaf temperature (Campbell & Norman, 2012) in BEPS:

$$LE_i = (VPD + \Delta(T_i - T_a))\rho c_p g_{W\_i}/\gamma \quad \text{(B15)}$$

where $i$, $\rho$ and $c_p$ have the same meaning as above, VPD is the vapor pressure deficit of the ambient air, $\gamma$ is the psychrometric constant, $\Delta$ is the slope of the saturation vapor pressure curve at air temperature, and $g_w$ is total conductance of water vapor from leaf interior to the atmosphere, which equals to the reciprocal of the tandem of the leaf boundary layer resistance, aerodynamic resistance, and leaf stomatal resistance ($1/g_s$). $g_s$ is obtained from the carbon assimilation module using Farquhar's model and the Ball-Woodrow-Berry equation.

Ultimately, the three components of leaf energy budget are expressed as a function of leaf temperature. We reiterate the processes above until the leaf temperature converge to realize the leaf energy balance.

Appendix C: Quantification of the Soil Water Stress Factor

To account for the effect of the soil water deficit on stomatal conductance, a soil water stress factor ($f_w$) based on the ratio of the measured available water in the soil to the maximum plant available water (Chen et al., 2005; Wang & Leuning, 1998; Wigmosta et al., 1994) was calculated as follows:

$$f_w = \begin{cases} 0 & \\ \dfrac{\theta_{sw}(z) - \theta_{wp}}{\theta_{fc} - \theta_{wp}} & \theta_{sw}(z) < \theta_{wp} \\ 1 & \theta_{wp} \le \theta_{sw}(z) \le \theta_{fc} \\ & \theta_{sw}(z) > \theta_{fc} \end{cases} \quad \text{(C1)}$$

where $\theta_{sw}(z)$ is the soil water content of layer $z$ and $z$ often refers to the top 30 cm based on the availability of the soil water measurements. $\theta_{wp}$ and $\theta_{fc}$ are the wilting point and the field capacity, respectively, ($m^3/m^3$) of the soil layer. $\theta_{wp}$ and $\theta_{fc}$ are derived from the soil texture information provided by Fluxnet (http://fluxnet.ornl.gov/), the patterns of multiyear soil moisture measurements and the algorithm developed by Saxton and Rawls (2006).

Appendix D: Parameterization for TBL

According to literature (Dai et al., 2004; Ryu et al., 2011; Wang & Leuning, 1998), TBL will upscale the leaf-level $V_{max}^{25}$ to its canopy counterpart first, then it will calculate $A_c$ and $G_s$ directly without the derivation of the parameter $A$ and $g_s$. In this case,

$$V^{25}_{\text{max\_canopy}} = \int_0^L V^{25}_{\text{max\_0}} \chi_n N(L) \mathrm{d}L \quad \text{(D1)}$$

$$V^{25}_{\text{max\_sunlit\_canopy}} = \int_0^L V^{25}_{\text{max\_0}} \chi_n N(L) f_{\text{sun}}(L) \mathrm{d}L \quad \text{(D2)}$$

$$V^{25}_{\text{max\_shaded\_canopy}} = V^{25}_{\text{max\_canopy}} - V^{25}_{\text{max\_sunlit\_canopy}} = \int_0^L V^{25}_{\text{max\_0}} \chi_n N(L) f_{\text{sh}}(L) \mathrm{d}L \quad \text{(D3)}$$

where $V^{25}_{\text{maxcanopy}}$, $V^{25}_{\text{maxsunlitcanopy}}$, and $V^{25}_{\text{maxshadedcanopy}}$ are the canopy-level $V^{25}_{\text{max}}$ for the whole canopy, sunlit canopy, and shaded canopy, respectively. $N(L)$ is the nitrogen gradient in canopy, and $f_{\text{sun}}(L)$and $f_{\text{sh}}(L)$ are the fraction of sunlit and shaded leaves in the canopy that change with the canopy depth (Appendix A).

Through using the canopy-scale $V^{25}_{max}$ in Farquhar's biochemical model and the Ball-Woodrow-Berry stomatal conductance model, we obtain the $G_s$ and $A_c$ for the sunlit canopy and shaded canopy, respectively.

## Appendix E: Correlations Between the Simulated Hourly ET (GPP) and Measured Hourly ET (GPP) Under All Schemes

Table E1 shows that on average, simulations using BL, TBL, and TL explains about 67%, 70%, and 71% of the variance in the ET measurements, respectively. Linear correlations between the simulations and the measurements indicate that TL performs best in capturing the temporal patterns of ET with a regression slope of 0.91, while BL and TBL underestimate ET with slopes of 0.72 and 0.83, respectively. Average root-mean-square errors (RMSEs) between simulated and measured ET are 0.055, 0.055 and 0.051 mm/h using BL, TBL, and TL, respectively.

**Table E1**
*Correlations Between the Simulated Hourly ET (GPP) and Measured Hourly ET (GPP) Under All Schemes*

| | | | ET | | | | GPP | | | |
|---|---|---|---|---|---|---|---|---|---|---|
| Site ID | Year | Upscaling schemes | $r^2$ | Slope | Intercept (mm/h) | RMSE (mm/h) | $r^2$ | Slope | Intercept (g/m$^2$/h) | RMSE (g/m$^2$/h) |
| CaCa2 | 2002–2010 | BL | 0.71 | 0.76 | 0.006 | 0.04 | 0.78 | 0.72 | 0.015 | 0.10 |
| | | TBL | 0.73 | 0.89 | 0.003 | 0.04 | 0.84 | 1.02 | 0.009 | 0.09 |
| | | TL | 0.74 | 0.92 | 0.004 | 0.04 | 0.85 | 0.98 | 0.015 | 0.08 |
| CaCa3 | 2002–2009 | BL | 0.69 | 0.71 | 0.007 | 0.05 | 0.72 | 0.69 | 0.018 | 0.14 |
| | | TBL | 0.72 | 0.84 | 0.004 | 0.05 | 0.84 | 1.05 | 0.013 | 0.12 |
| | | TL | 0.76 | 0.98 | 0.005 | 0.04 | 0.84 | 0.99 | 0.016 | 0.11 |
| CaCbo | 2008–2013 | BL | 0.55 | 0.52 | 0.025 | 0.09 | 0.65 | 0.62 | 0.047 | 0.22 |
| | | TBL | 0.65 | 0.62 | 0.021 | 0.08 | 0.77 | 0.89 | 0.052 | 0.18 |
| | | TL | 0.65 | 0.71 | 0.023 | 0.08 | 0.78 | 0.87 | 0.054 | 0.18 |
| CaGro | 2005–2011 | BL | 0.69 | 0.76 | 0.016 | 0.05 | 0.77 | 0.66 | 0.011 | 0.13 |
| | | TBL | 0.72 | 0.89 | 0.011 | 0.06 | 0.82 | 0.92 | 0.007 | 0.11 |
| | | TL | 0.73 | 0.94 | 0.011 | 0.05 | 0.84 | 0.90 | 0.009 | 0.10 |
| CaOas | 2002–2010 | BL | 0.73 | 0.80 | 0.013 | 0.05 | 0.82 | 0.82 | 0.017 | 0.12 |
| | | TBL | 0.79 | 0.89 | 0.010 | 0.05 | 0.90 | 0.98 | 0.006 | 0.09 |
| | | TL | 0.80 | 0.91 | 0.009 | 0.05 | 0.90 | 0.98 | 0.011 | 0.09 |
| CaObs | 2002–2009 | BL | 0.62 | 0.89 | 0.015 | 0.06 | 0.61 | 0.68 | 0.006 | 0.11 |
| | | TBL | 0.62 | 1.03 | 0.012 | 0.06 | 0.67 | 0.99 | −0.001 | 0.11 |
| | | TL | 0.65 | 1.08 | 0.012 | 0.06 | 0.69 | 0.96 | 0.005 | 0.11 |
| CaOjp | 2005–2010 | BL | 0.57 | 0.67 | 0.020 | 0.04 | 0.69 | 0.63 | 0.011 | 0.08 |
| | | TBL | 0.57 | 0.74 | 0.019 | 0.05 | 0.67 | 0.82 | 0.008 | 0.08 |
| | | TL | 0.57 | 0.76 | 0.020 | 0.05 | 0.72 | 0.85 | 0.013 | 0.07 |
| CaTp3 | 2009–2013 | BL | 0.74 | 0.65 | 0.016 | 0.05 | 0.82 | 0.54 | 0.034 | 0.17 |
| | | TBL | 0.77 | 0.78 | 0.011 | 0.04 | 0.88 | 0.87 | 0.046 | 0.11 |
| | | TL | 0.79 | 0.90 | 0.012 | 0.04 | 0.88 | 0.80 | 0.045 | 0.11 |
| CaTp4 | 2008–2013 | BL | 0.71 | 0.68 | 0.010 | 0.06 | 0.82 | 0.60 | 0.019 | 0.15 |
| | | TBL | 0.73 | 0.75 | 0.007 | 0.06 | 0.89 | 0.98 | 0.027 | 0.11 |
| | | TL | 0.74 | 0.95 | 0.006 | 0.06 | 0.89 | 0.87 | 0.025 | 0.10 |

In the linear regressions between simulated GPP and measured GPP, the mean $r^2$ values are 0.69, 0.81, and 0.82, and the mean slopes are 0.66, 0.95, and 0.92 for BL, TBL, and TL, respectively. Moreover, the mean RMSEs are 0.135, 0.112, and 0.107 $g/m^2/h$ for BL, TBL, and TL, respectively. TBL and TL simulate GPP with similar accuracies, while BL significantly underestimates GPP. The variations of these statistics across the sites are smaller for TL or TBL than for BL, suggesting that TL or TBL is more suitable for large-scale applications.

References


Alton, P. B., Ellis, R., Los, S. O., & North, P. R. (2007). Improved global simulations of gross primary product based on a separate and explicit treatment of diffuse and direct sunlight. *Journal of Geophysical Research*, 112, D07203. https://doi.org/10.1029/2006JD008022

Amthor, J. S. (1994). Scaling $CO_2$ photosynthesis relationships from the leaf to the canopy. *Photosynthesis Research*, 39( 3), 321– 350. https://doi.org/10.1007/BF00014590

Amthor, J. S., Chen, J. M., Clein, J. S., Frolking, S. E., Goulden, M. L., Grant, R. F., … Wofsy, S. C. (2001). Boreal forest $CO_2$ exchange and evapotranspiration predicted by nine ecosystem process models: Intermodel comparisons and relationships to field measurements. *Journal of Geophysical Research*, 106( D24), 33,623– 33,648. https://doi.org/10.1029/2000JD900850

Arain, M. A., & Restrepo-Coupe, N. (2005). Net ecosystem production in a temperate pine plantation in southeastern Canada. *Agricultural and Forest Meteorology*, 128, 223– 241. https://doi.org/10.1016/j.agrformet.2004.10.003

Baldocchi, D. (1994). An analytical solution for coupled leaf photosynthesis and stomatal conductance models. *Tree Physiology*, 14( 7-8-9), 1069– 1079. https://doi.org/10.1093/treephys/14.7-8-9.1069

Baldocchi, D., & Meyers, T. (1998). On using eco-physiological, micrometeorological and biogeochemical theory to evaluate carbon dioxide, water vapor and trace gas fluxes over vegetation: A perspective. *Agricultural and Forest Meteorology*, 90( 1-2), 1– 25. https://doi.org/10.1016/S0168-1923(97)00072-5

Baldocchi, D. D., & Harley, P. C. (1995). Scaling carbon dioxide and water vapour exchange from leaf to canopy in a deciduous forest. II. Model testing and application. *Plant, Cell and Environment*, 18( 10), 1157– 1173. https://doi.org/10.1111/j.1365-3040.1995.tb00626.x

Ball, J. T., Woodrow, I. E., & Berry, J. A. (1987). A Model predicting stomatal conductance and its contribution to the control of photosynthesis under different environmental conditions. In J. Biggins (Ed.) *Progress in photosynthesis research: Volume 4 Proceedings of the VIIth International Congress on Photosynthesis Providence* (pp. 221– 224). August 10–15, 1986.

Rhode Island, Dordrecht, Netherlands: Springer Netherlands, Dordrecht. https://doi.org/10.1007/978-94-017-0519-6_48

Barr, A. G., Black, T. A., Hogg, E. H., Kljun, N., Morgenstern, K., & Nesic, Z. (2004). Inter-annual variability in the leaf area index of a boreal aspen-hazelnut forest in relation to net ecosystem production. *Agricultural and Forest Meteorology*, 126, 237– 255. https://doi.org/10.1016/j.agrformet.2004.06.011

Barr, A. G., Morgenstern, K., Black, T. A., McCaughey, J. H., & Nesic, Z. (2006). Surface energy balance closure by the eddy-covariance method above three boreal forest stands and implications for the measurement of the CO2 flux. *Agricultural and Forest Meteorology*, 140, 322– 337. https://doi.org/10.1016/j.agrformet.2006.08.007

Bergeron, O., Margolis, H. A., Black, T. A., Coursolle, C., Dunn, A. L., Barr, A. G., & Wofsy, S. C. (2007). Comparison of carbon dioxide fluxes over three boreal black spruce forests in Canada. *Global Change Biology*, 13, 89– 107. https://doi.org/10.1111/j.1365-2486.2006.01281.x

Bonan, G. B. (1996). Ecological, hydrological, and atmospheric studies: Technical description and user's guide.

Brutsaert, W. (1982). *Evaporation Into the Atmosphere*. Dordrecht, Netherlands: Springer. https://doi.org/10.1007/978-94-017-1497-6

Campbell, G. S., & Norman, J. M. (2012). *An introduction to environmental biophysics. An introduction to environmental biophysics* (Vol. 6). Springer-Verlag New York: Springer Science & Business Media.

Chen, B., Black, T. A., Coops, N. C., Hilker, T., Trofymow, J. A., & Morgenstern, K. (2009). Assessing tower flux footprint climatology and scaling between remotely sensed and eddy covariance measurements. *Boundary-Layer Meteorology*, 130, 137– 167. https://doi.org/10.1007/s10546-008-9339-1

Chen, B., Chen, J. M., & Ju, W. (2007). Remote sensing-based ecosystem-atmosphere simulation scheme (EASS)—Model formulation and test with multiple-year data. *Ecological Modelling*, 209, 277– 300. https://doi.org/10.1016/j.ecolmodel.2007.06.032

Chen, J. M., Chen, X., Ju, W., & Geng, X. (2005). Distributed hydrological model for mapping evapotranspiration using remote sensing inputs. *Journal of Hydrology*, 305, 15– 39. https://doi.org/10.1016/j.jhydrol.2004.08.029

Chen, J. M., Govind, A., Sonnentag, O., Zhang, Y., Barr, A., & Amiro, B. (2006). Leaf area index measurements at Fluxnet-Canada forest sites. *Agricultural and Forest Meteorology*, 140, 257– 268. https://doi.org/10.1016/j.agrformet.2006.08.005

Chen, J. M., Liu, J., Cihlar, J., & Goulden, M. (1999). Daily canopy photosynthesis model through temporal and spatial scaling for remote

sensing applications. *Ecological Modelling*, 124( 2-3), 99– 119. https://doi.org/10.1016/S0304-3800(99)00156-8

Chen, J. M., Mo, G., Pisek, J., Liu, J., Deng, F., Ishizawa, M., & Chan, D. (2012). Effects of foliage clumping on the estimation of global terrestrial gross primary productivity. *Global Biogeochemical Cycles*, 26, GB1019. https://doi.org/10.1029/2010GB003996

Chen, J. M., Rich, P. M., Gower, S. T., Norman, J. M., & Plummer, S. (1997). Leaf area index of boreal forests: Theory, techniques, and measurements. *Journal of Geophysical Research*, 102( D24), 29429. https://doi.org/10.1029/97JD01107

Chen, J. M., Yang, B. J., & Zhang, R. H. (1989). Soil thermal emissivity as affected by its water content and surface treatment. *Soil Science*, 148( 6), 433– 435. https://doi.org/10.1097/00010694-198912000-00005

Chen, J. M., & Zhang, R. H. (1989). Studies on the measurements of crop emissivity and sky temperature. *Agricultural and Forest Meteorology*, 49( 1), 23– 34. https://doi.org/10.1016/0168-1923(89)90059-2

Cramer, W., Bondeau, A., Woodward, F. I., Prentice, I. C., Betts, R. A., Brovkin, V., ... Young-Molling, C. (2001). Global response of terrestrial ecosystem structure and function to $CO_2$ and climate change: Results from six dynamic global vegetation models. *Global Change Biology*, 7( 4), 357–373. https://doi.org/10.1046/j.1365-2486.2001.00383.x

Croft, H., Chen, J. M., Froelich, N. J., Chen, B., & Staebler, R. M. (2015). Seasonal controls of canopy chlorophyll content on forest carbon uptake: Implications for GPP modeling. *Journal of Geophysical Research: Biogeosciences*, 120, 1576– 1586. https://doi.org/10.1002/2015JG002980

Dai, Y., Dickinson, R. E., & Wang, Y.-P. (2004). A two-big-leaf model for canopy temperature, photosynthesis, and stomatal conductance. *Journal of Climate*, 17( 12), 2281– 2299. https://doi.org/10.1175/1520-0442(2004)017%3C2281:ATMFCT%3E2.0.CO;2

De Pury, D. G. G., & Farquhar, G. D. (1997). Simple scaling of photosynthesis from leaves to canopies without the errors of big-leaf models. *Plant, Cell and Environment*, 20( 5), 537– 557. https://doi.org/10.1111/j.1365-3040.1997.00094.x

Dickinson, E., A. Henderson-Sellers, and J. Kennedy (1993). Biosphere-atmosphere Transfer Scheme (BATS) version 1e as coupled to the NCAR Community Climate Model, *NCAR Tech. Rep. NCAR/TN-3871STR, 72*, (August), 77, doi:10.5065/D67W6959.

Dickinson, R. E., Henderson-Sellers, A., Rosenzweig, C., & Sellers, P. J. (1991). Evapotranspiration models with canopy resistance for use in climate models: A review. *Agricultural and Forest Meteorology*, 54( 2-4), 373– 388. https://doi.org/10.1016/0168-1923(91)90014-H

Farquhar, G. D., von Caemmerer, S., & Berry, J. A. (1980). A biochemical model of photosynthetic $CO_2$ assimilation in leaves of $C_3$ species. *Planta*, 149( 1), 78– 90. https://doi.org/10.1007/BF00386231

Friend, A. D. (2001). Modelling canopy $CO_2$ fluxes: Are “big-leaf” simplifications justified? *Global Ecology and Biogeography*, 10( 6), 603– 619. https://doi.org/10.1046/j.1466-822x.2001.00268.x

Froelich, N., Croft, H., Chen, J. M., Gonsamo, A., & Staebler, R. M. (2015). Trends of carbon fluxes and climate over a mixed temperate–boreal transition forest in southern Ontario, Canada. *Agricultural and Forest Meteorology*, 211-212, 72– 84. https://doi.org/10.1016/j.agrformet.2015.05.009

Gökkaya, K., Thomas, V., Noland, T., McCaughey, H., & Treitz, P. (2013). Testing the robustness of predictive models for chlorophyll generated from spaceborne imaging spectroscopy data for a mixedwood boreal forest canopy. *International Journal of Remote Sensing*, 35( 1), 218– 233. https://doi.org/10.1080/01431161.2013.866291

Gonsamo, A., & Chen, J. M. (2014). Continuous observation of leaf area index at Fluxnet-Canada sites. *Agricultural and Forest Meteorology*, 189-190, 168– 174. https://doi.org/10.1016/j.agrformet.2014.01.016

Gonsamo, A., Chen, J. M., Price, D. T., Kurz, W. a., Liu, J., Boisvenue, C., … Chang, K. H. (2013). Improved assessment of gross and net primary productivity of Canada's landmass. *Journal of Geophysical Research: Biogeosciences*, 118, 1546– 1560. https://doi.org/10.1002/2013JG002388

Grant, R. F., Zhang, Y., Yuan, F., Wang, S., Hanson, P. J., Gaumont-Guay, D., … Arain, A. (2006). Intercomparison of techniques to model water stress effects on $CO_2$ and energy exchange in temperate and boreal deciduous forests. *Ecological Modelling*, 196, 289– 312. https://doi.org/10.1016/j.ecolmodel.2006.02.035

Groenendijk, M., Dolman, A. J., Ammann, C., Arneth, A., Cescatti, A., Dragoni, D., … Wohlfahrt, G. (2011). Seasonal variation of photosynthetic model parameters and leaf area index from global Fluxnet eddy covariance data. *Journal of Geophysical Research*, 116, G04027. https://doi.org/10.1029/2011JG001742

He, L., Chen, J. M., Liu, J., Mo, G., Bélair, S., Zheng, T., … Barr, A. G. (2014). Optimization of water uptake and photosynthetic parameters in an ecosystem model using tower flux data. *Ecological Modelling*, 294, 94– 104. https://doi.org/10.1016/j.ecolmodel.2014.09.019

He, L., Chen, J. M., Pisek, J., Schaaf, C. B., & Strahler, A. H. (2012). Global clumping index map derived from the MODIS BRDF product. *Remote Sensing of Environment*, 119, 118– 130. https://doi.org/10.1016/j.rse.2011.12.008

Ju, W., Chen, J. M., Black, T. A., Barr, A. G., Liu, J., & Chen, B. (2006). Modelling multi-year coupled carbon and water fluxes in a boreal aspen

forest. *Agricultural and Forest Meteorology*, 140, 136– 151. https://doi.org/10.1016/j.agrformet.2006.08.008

Kelliher, F. M., Leuning, R., Raupach, M. R., & Schulze, E.-D. (1995). Maximum conductances for evaporation from global vegetation types. *Agricultural and Forest Meteorology*, 73( 1-2), 1– 16. https://doi.org/10.1016/0168-1923(94)02178-M

Lai, C.-T., Katul, G., Oren, R., Ellsworth, D., & Schäfer, K. (2000). Modeling $CO_2$ and water vapor turbulent flux distributions within a forest canopy. *Journal of Geophysical Research*, 105( D21), 26,333– 26,351. https://doi.org/10.1029/2000JD900468

Leuning, R. (1990). Modelling stomatal behaviour and and photosynthesis of *Eucalyptus grandis*. *Australian Journal of Plant Physiology*, 17( 2), 159– 175. https://doi.org/10.1071/PP9900159

Leuning, R., Kelliher, F. M., De Pury, D. G. G., & Schulze, E.-D. (1995). Leaf nitrogen, photosynthesis, conductance and transpiration: Scaling from leaves to canopies. *Plant, Cell and Environment*, 18( 10), 1183– 1200. https://doi.org/10.1111/j.1365-3040.1995.tb00628.x

Liu, J., Chen, J. M., & Cihlar, J. (2003). Mapping evapotranspiration based on remote sensing: An application to Canada's landmass. *Water Resources Research*, 39( 7), 1189. https://doi.org/10.1029/2002WR001680

Medlyn, B., Barrett, D., Landsberg, J., Sands, P., & Clement, R. (2003). Conversion of canopy intercepted radiation to photosynthate: review of modelling approaches for regional scales. *Functional Plant Biology*, 30( 2), 153. https://doi.org/10.1071/FP02088

Medlyn, B. E., Badeck, F. W., de Pury, D. G. G., Barton, C. V. M., Broadmeadow, M., Ceulemans, R., … Jstbid, P. G. (1999). Effects of elevated [$CO_2$] on photosynthesis in European forest species: a meta-analysis of model parameters. *Plant, Cell & Environment*, 22( 12), 1475– 1495. https://doi.org/10.1046/j.1365-3040.1999.00523.x

Medlyn, B. E., Duursma, R. A., Eamus, D., Ellsworth, D. S., Prentice, I. C., Barton, C. V. M., … Wingate, L. (2011). Reconciling the optimal and empirical approaches to modelling stomatal conductance. *Global Change Biology*, 17, 2134– 2144. https://doi.org/10.1111/j.1365-2486.2010.02375.x

Mercado, L., Lloyd, J., Carswell, F., Malhi, Y., Meir, P., & Nobre, A. D. (2006). Modelling Amazonian forest eddy covariance data: a comparison of big leaf versus sun/shade models for the C-14 tower at Manaus I. Canopy photosynthesis. *Acta Amazonica*, 36, 69– 82. https://doi.org/10.1590/S0044-59672006000100009

Monteith, J. L., & Unsworth, M. H. (2013). *Principles of Environmental Physics*. Amsterdam, Netherlands: Elsevier.

Moran, M. S., Rahman, A. F., Washburne, J. C., Goodrich, D. C., Weltz, M. A., & Kustas, W. P. (1996). Combining the Penman-Monteith equation with measurements of surface temperature and reflectance to estimate evaporation rates of semiarid grassland. *Agricultural and Forest Meteorology*, 80( 2-4), 87– 109. https://doi.org/10.1016/0168-1923(95)02292-9

Mu, Q., Zhao, M., & Running, S. W. (2011). Improvements to a MODIS global terrestrial evapotranspiration algorithm. *Remote Sensing of Environment*, 115( 8), 1781– 1800. https://doi.org/10.1016/j.rse.2011.02.019

Norman, J. M. (1982). *Biometeorology in Integrated Pest Management*. New York: Elsevier.

Norman, J. M., Kustas, W. P., & Humes, K. S. (1995). Source approach for estimating soil and vegetation energy fluxes in observations of directional radiometric surface temperature. *Agricultural and Forest Meteorology*, 77( 3-4), 263– 293. https://doi.org/10.1016/0168-1923(95)02265-Y

Oki, T., & Kanae, S. (2006). Global hydrological cycles and world water resources. *Science*, 313, 1068– 1072. https://doi.org/10.1126/science.1128845

Paw, U. K., & Meyers, T. P. (1989). Investigations with a higher-order canopy turbulence model into mean source-sink levels and bulk canopy resistances. *Agricultural and Forest Meteorology*, 47( 2-4), 259– 271. https://doi.org/10.1016/0168-1923(89)90099-3

Peichl, M., Brodeur, J. J., Khomik, M., & Arain, M. A. (2010). Biometric and eddy-covariance based estimates of carbon fluxes in an age-sequence of temperate pine forests. *Agricultural and Forest Meteorology*, 150, 952– 965. https://doi.org/10.1016/j.agrformet.2010.03.002

Phillips, N., & Oren, R. (1998). A comparison of daily representations of canopy conductance based on two conditional time-averaging methods and the dependence of daily conductance on environmental factors. *Annales des Sciences Forestières*, 55( 1-2), 217– 235. https://doi.org/10.1051/forest:19980113

Potter, C. S., Wang, S., Nikolov, N. T., McGuire, A. D., Liu, J., King, A. W., … Amthor, J. S. (2001). Comparison of boreal ecosystem model sensitivity to variability in climate and forest site parameters. *Journal of Geophysical Research*, 106( D24), 33671– 33687. https://doi.org/10.1029/2000JD000224

Raupach, M., & Finnigan, J. (1988). Single-layer models of evaporation from plant canopies are incorrect but useful, whereas multilayer models are correct but useless: Discuss. *Australian Journal of Plant Physiology*, 15( 6), 705. https://doi.org/10.1071/PP9880705

Ryu, Y., Baldocchi, D. D., Kobayashi, H., van Ingen, C., Li, J., Black, T. A., … Roupsard, O. (2011). Integration of MODIS land and atmosphere products with a coupled-process model to estimate gross primary productivity and

evapotranspiration from 1 km to global scales. *Global Biogeochemical Cycles*, 25, GB4017. https://doi.org/10.1029/2011GB004053

Sala, A., & Tenhunen, J. D. (1996). Simulations of canopy net photosynthesis and transpiration in *Quercus ilex* L. under the influence of seasonal drought. *Agricultural and Forest Meteorology*, 78( 3-4), 203– 222. https://doi.org/10.1016/0168-1923(95)02250-3

Saxton, K. E., & Rawls, W. J. (2006). Soil water characteristic estimates by texture and organic matter for hydrologic solutions. *Soil Science Society of America Journal*, 70, 1569. https://doi.org/10.2136/sssaj2005.0117

Sellers, P. J. (1997). Modeling the Exchanges of Energy, Water, and Carbon Between Continents and the Atmosphere. *Science*, 275( 5299), 502– 509. https://doi.org/10.1126/science.275.5299.502

Sellers, P. J., Berry, J. A., Collatz, G. J., Field, C. B., & Hall, F. G. (1992). Canopy reflectance, photosynthesis, and transpiration. III. A reanalysis using improved leaf models and a new canopy integration scheme. *Remote Sensing of Environment*, 42( 3), 187– 216. https://doi.org/10.1016/0034-4257(92)90102-P

Sellers, P. J., Mintz, Y., Sud, Y. C., & Dalcher, A. (1986). A simple biosphere model (SiB) for use within general circulation models. *Journal of Atmospheric Science*, 43( 6), 505– 531. https://doi.org/10.1175/1520-0469(1986)043%3C0505:ASBMFU%3E2.0.CO;2

Sinclair, T. R., Murphy, C. E., & Knoerr, K. R. (1976). Development and evaluation of simplified models for simulating canopy photosynthesis and transpiration. *Journal of Applied Ecology*, 13( 3), 813– 829. https://doi.org/10.2307/2402257

Sprintsin, M., Chen, J. M., Desai, A., & Gough, C. M. (2012). Evaluation of leaf-to-canopy upscaling methodologies against carbon flux data in North America. *Journal of Geophysical Research*, 117, G01023. https://doi.org/10.1029/2010JG001407

Stewart, J. (1988). Modelling surface conductance of pine forest. *Agricultural and Forest Meteorology*, 43( 1), 19– 35. https://doi.org/10.1016/0168-1923(88)90003-2

Trenberth, K. E., Fasullo, J. T., & Kiehl, J. (2009). Earth's global energy budget. *Bulletin of the American Meteorological Society*, 90, 311– 323. https://doi.org/10.1175/2008BAMS2634.1

Vogel, C. a., Baldocchi, D. D., Luhar, A. K., & Rao, K. S. (1995). A Comparison of a hierarchy of models for determining energy balance components over vegetation canopies. *Journal of Applied Meteorology*. https://doi.org/10.1175/1520-0450(1995)034<2182:ACOAHO>2.0.CO;2

Wang, H., Prentice, I. C., Davis, T. W., Keenan, T. F., Wright, I. J., & Peng, C. (2017). Photosynthetic responses to altitude: An explanation based on

optimality principles. *New Phytologist*, 213( 3), 976– 982. https://doi.org/10.1111/nph.14332

Wang, K., & Dickinson, R. E. (2012). A review of global terrestrial evapotranspiration: observation, modelling, climatology, and climatic variability. *Reviews of Geophysics*, 50, RG2005. https://doi.org/10.1029/2011RG000373

Wang, Q., Tenhunen, J., Falge, E., Bernhofer, C., Granier, A., & Vesala, T. (2004). Simulation and scaling of temporal variation in gross primary production for coniferous and deciduous temperate forests. *Global Change Biology*, 10, 37– 51. https://doi.org/10.1111/j.1365-2486.2003.00716.x

Wang, Y.-P., & Leuning, R. (1998). A two-leaf model for canopy conductance, photosynthesis and partitioning of available energy I. *Agricultural and Forest Meteorology*, 91( 1-2), 89– 111. https://doi.org/10.1016/S0168-1923(98)00061-6

Weiß, M., & Menzel, L. (2008). A global comparison of four potential evapotranspiration equations and their relevance to stream flow modelling in semi-arid environments. *Advances in Geosciences*, 18, 15– 23. https://doi.org/10.5194/adgeo-18-15-2008

Wigmosta, M. S., Vail, L. W., & Lettenmaier, D. P. (1994). A distributed hydrology-vegetation model for complex terrain. *Water Resources Research*, 30( 6), 1665– 1679. https://doi.org/10.1029/94WR00436

Xu, L., & Baldocchi, D. D. (2003). Seasonal trends in photosynthetic parameters and stomatal conductance of blue oak (*Quercus douglasii*) under prolonged summer drought and high temperature. *Tree Physiology*, 23( 13), 865– 877. https://doi.org/10.1093/treephys/23.13.865

Yan, H., Wang, S. Q., Billesbach, D., Oechel, W., Zhang, J. H., Meyers, T., … Scott, R. (2012). Global estimation of evapotranspiration using a leaf area index-based surface energy and water balance model. *Remote Sensing of Environment*, 124, 581– 595. https://doi.org/10.1016/j.rse.2012.06.004